



Copper complexes induce haem oxygenase-1 (HMOX1) and cause apoptotic cell death in pancreatic cancer cells

Zakeeya Jhetam^a, Carla Martins-Furness^a, Cathy Slabber^b, Orde Q. Munro^{b,c}, Marietha Nel^d, Leonie Harmse^{a,*}

^a Division of Pharmacology, Department of Pharmacy and Pharmacology, Faculty of Health Sciences, University of the Witwatersrand, 7 York Road, Parktown 2193, South Africa

^b Molecular Sciences Institute, School of Chemistry, University of the Witwatersrand, 1 Jan Smut Ave, Braamfontein, Johannesburg 2017, South Africa

^c School of Chemistry, University of Leeds, Woodhouse Lane, Leeds LS2 9JT, UK

^d Dept of Surgery, Faculty of Health Sciences, University of the Witwatersrand, 7 York Road, Parktown 2193, South Africa

ARTICLE INFO

Keywords:

Pancreatic cancer
Haem oxygenase-1
Copper complexes
Intrinsic apoptosis

ABSTRACT

Pancreatic ductal adenocarcinoma (PDAC), the most common pancreatic malignancy, has a dismal 5-year survival rate, making palliative chemotherapy the only treatment option. Targeted therapy has limited efficacy in PDAC, underscoring the need for novel therapeutic approaches. The inducible stress-response protein, haem oxygenase-1 (HMOX1), has been implicated in treatment failure in PDAC.

Copper coordination complexes have shown promise as anticancer agents against various cancers, and are associated with apoptotic cell death. The different ligands to which copper is complexed, determine the specificity and efficacy of each complex.

Three different classes of copper complexes were evaluated for anti-cancer activity against AsPC-1 and MIA PaCa-2 pancreatic cancer cell lines. A copper-phenanthroline-theophylline complex (CuPhTh₂), a copper-8-aminoquinoline-naphthyl complex (Cu8AqN), and two copper-aromatic-isoindoline complexes (CuAIsI) were effective inhibitors of cell proliferation with clinically relevant IC₅₀ values below 5 μM. The copper complexes caused reactive oxygen species (ROS) formation, promoted annexin-V binding, disrupted the mitochondrial membrane potential (MMP) and activated caspase-9 and caspase-3/7, confirming apoptotic cell death.

Expression of nuclear HMOX1 was increased in both cell lines, with the CuPhTh₂ complex being the most active. Inhibition of HMOX1 activity significantly decreased the IC₅₀ values of these copper complexes suggesting that HMOX1 inhibition may alter treatment outcomes in PDAC.

1. Introduction

Pancreatic cancer is typically diagnosed at an advanced stage and is known for its poor prognosis [1]. Globally, it is ranked as the seventh leading cause of cancer-related mortality with 467,409 recorded deaths in 2022 [2]. Pancreatic ductal adenocarcinoma (PDAC), the most frequently diagnosed subtype of pancreatic cancer, is an exocrine tumour which originates in the epithelial lining of the pancreatic duct [3]. Diagnosis of PDAC is often made at a late and unresectable stage,

with 5-year survival rates varying between 3.2% and 16.2%, depending on the stage at first diagnosis [3,4].

In PDAC, mutations associated with tumour progression and promotion of metastasis are present in the *KRAS*, *CDKN2A*, *TP53* and *SMAD4/DPC4* genes [5,6]. Mutations in *KRAS* are present in 95% of PDAC patients resulting in the synthesis of a constitutively active *KRAS* kinase, an oncogenic driver of tumorigenesis [7–9].

Mutations in *CDKN2A* are present in nearly 98% of PDAC patients and inactivate p16, a cyclin-dependent kinase inhibitor which allows

Abbreviations: AO, Acridine orange; AU, Arbitrary Units; cIAP1, Cellular inhibitor of apoptosis protein-1; HMOX-1, Haem oxygenase 1; HTRA (OMI), High temperature requirement protein A2; HO, Hoechst 33342; HAS, Human serum albumin; IAPs, Inhibitor of Apoptosis Proteins; JC-1, 1,1',3,3'-Tetraethyl-5,5',6,6'-tetrachloroimidacarbocyanine iodide; MDM2, Mouse double minute 2 homolog; MTT, 3-(4,5-dimethylthiazol-2-yl)-2,5-diphenyltetrazolium bromide; NF-κB, Nuclear factor kappa B; OB24, 1-[[2-[2-(4-Bromophenyl)ethyl]-1,3-dioxolan-2-yl]methyl]-1H-imidazole.HCl; PC, Phase contrast; PBS, Phosphate buffered saline; Smac/Diablo, Second mitochondria-derived activator of caspase; TNFR1, Tumour necrosis factor receptor 1; XIAP, X-linked inhibitor of apoptosis protein.

* Corresponding author.

E-mail address: Leonie.Harmse@wits.ac.za (L. Harmse).

<https://doi.org/10.1016/j.jinorgbio.2024.112815>

Received 27 July 2024; Received in revised form 14 December 2024; Accepted 15 December 2024

Available online 18 December 2024

0162-0134/© 2024 The Authors. Published by Elsevier Inc. This is an open access article under the CC BY-NC-ND license (<http://creativecommons.org/licenses/by-nc-nd/4.0/>).

progression of the cell cycle. [10–13]. Approximately 70 % of PDAC patients have mutations in *TP53*, resulting in the synthesis of a mutant p53 protein which either lacks tumour suppressor function, or is a mutant p53 protein that promotes the survival and proliferation of tumour cells [14,15]. SMAD4 is activated in response to Transforming Growth Factor beta (TGF- β) signaling [16], and is inactivated in close to 50 % of PDAC cases [17,18]. The SMAD4/TGF- β pathway promotes cell cycle arrest, apoptosis and DNA repair [16].

The presence of multiple mutations in multiple signal transduction pathways makes targeted treatment of PDAC elusive with minimal successes. Targeted treatments, including immune checkpoint inhibitors offer a short-lived benefit to PDAC patients with the rapid development of resistance contributing to treatment failure [19,20].

Surgical resection followed by adjuvant chemotherapy is the standard of care when patients are diagnosed with early stage, resectable pancreatic cancer [21]. Unfortunately, only 15–20 % of patients are eligible for resection and in many of these patients the cancer recurs due to the presence of undetectable micro-metastases [19,22].

In patients with metastatic disease, treatment regimens are determined on a patient specific basis, with chemoradiation being frequently used. Chemotherapy comprises gemcitabine, paclitaxel, 5-fluorouracil or capecitabine, irinotecan and platinum-based drugs like cisplatin or oxaliplatin. Regimens consisting of 5-fluorouracil /folinic acid plus oxaliplatin and irinotecan (FOLFIRINOX) or gemcitabine plus nano-albumin-bound (nab)-paclitaxel are currently the first-line treatment options for patients with low morbidity scores [21]. As patients deteriorate, palliative treatment includes gemcitabine monotherapy or a combination of gemcitabine with capecitabine [20,22]. All these drugs cause serious adverse effects and contribute to patient morbidity while offering a meagre survival benefit.

While the use of targeted therapy like pembrolizumab is beneficial in select patients, they make up a small percentage of the total number of PDAC cases [23]. Additionally, the current cost of targeted treatments renders them a non-viable standard-of-care treatment option for the majority of patients. There is thus a clear need to find alternative treatments for pancreatic cancer.

The transition metal, copper, has gained much attention as an alternative to platinum-based chemotherapeutic agents in the potential treatment of a wide variety of cancers. Platinum-based drugs are widely used in cancer treatment regimens but are hindered by instability in aqueous media and the rapid development of resistance or the presence of innate resistance and unresponsiveness in patients. The platinum-based drugs are known for serious adverse drug reactions like nephro-, oto- and neuro-toxicity [24]. Copper is a micronutrient and an essential co-factor for a number of important biochemical reactions catalyzed by cytochrome *c* oxidase, superoxide dismutase, lysyl oxidase, dopamine- β oxygenase and tyrosinase [25,26]. Apart from these enzymes, copper is important for the activity of a number of oxidases such as ascorbate-oxidase, amine-oxidase, galactose-oxidase and phenol-oxidase [25,26].

Copper homeostasis is tightly regulated and a disruption, in the form of exogenous organic copper molecules, may be detrimental to tumour cells [27]. In addition, the general consensus is that endogenous homeostatic mechanisms exist to regulate copper levels, and these same mechanisms will afford some protection against the adverse effects of a copper overload.

Copper has been complexed to various classes of organic ligands and these complexes have shown a wide variation in their potential as effective anticancer agents [28]. The organic ligand plays an important role in the ability of the complex to enter cells and may contribute to the potency, efficacy and toxicity of the specific copper complex [29]. For example $[\text{Cu}(\text{dmp})_2(\text{CH}_3\text{CN})]^{2+}$ was proven superior to $[\text{Cu}(\text{phen})_2(\text{CH}_3\text{CN})]^{2+}$ and cisplatin in inducing cytotoxicity and antitumor activity in bone, lung, and breast cancer cell lines [30]. This was confirmed when $[\text{Cu}(\text{dmp})_2(\text{CH}_3\text{CN})]^{2+}$ was shown to be superior to $[\text{Cu}(\text{phen})_2(\text{CH}_3\text{CN})]^{2+}$ when tested in three colorectal cancer cell lines [31]. However, the identification of the specific molecular targets of the

numerous types of copper complexes remains elusive [28,29].

Mechanisms of action of copper complexes currently described in the literature include the induction of reactive oxygen species (ROS) and oxidative stress, [32] a disruption of mitochondrial function [33,34] and, the inhibition of angiogenesis by decreasing VEGF expression [35]. There are numerous reports regarding the binding of copper complexes to DNA either by intercalation or groove binding [28,29,36]. In addition, copper complexes have been shown to directly cleave DNA via a ROS mediated mechanism [37], or indirectly by the inhibition of topoisomerases [38]. Inhibition of the proteasome has emerged as an additional mechanism of action of copper(II)-Schiff base complexes [39,40]. The ability of the complexes to generate ROS impaired the function of the proteasome, in addition to causing mitochondrial and DNA damage [40]. Inhibition of the proteolytic function of the proteasome results in the accumulation of ubiquitinated proteins, leading to cell death by apoptosis [39,40].

The *in vitro* anticancer activity of copper (II) complexed with different thiosemicarbazone ligands, was evaluated over a 72-h period on cell lines representing colorectal, pancreatic, thyroid and ovarian cancers, as well as melanoma [41,42]. The complexes showed a range of effectiveness with the most promising complexes being active in the low nanomolar range. The salicylate thiosemicarbazone complexes inhibited the function of the copper-binding protein disulfide isomerase, a newly identified chemotherapeutic target [41].

More recently Balsa *et al.*, 2023, [43] compared the proteome profiles of a triple negative breast cancer cell line which was treated with two copper(II)-hydrazone complexes. They observed significant changes in the proteome pertaining to endoplasmic reticulum stress, and the unfolded protein response. A downregulation of proteins involved in DNA replication and repair was observed. Intriguingly, there was a decrease in the mutant gain of function p53 protein which corroborates our earlier observation in HT-29 cells [44].

Moreover, copper complexes can be functionalized with specific ligands to target receptors that are overexpressed in specific cancers [45,46]. Copper complexes conjugated with a *N*-methyl-D-aspartate (NMDA) receptor antagonist were effective inhibitors of proliferation in a variety of cell lines at low micromolar concentrations [45]. In another study, copper complexes were functionalized with oestrogen and were effective inhibitors of oestrogen-receptor-positive breast cancer cell proliferation [46].

Many studies on novel copper complexes do not report details regarding the mechanism of cell death, which is an important aspect of new drug development. Necrotic cell death is not prudent as a mode of death in cancer treatment. It increases the risk for severe tumour lysis syndrome and contributes to patient morbidity [47]. Thus, it is of high importance that new investigational cancer agents do not cause necrotic cell death in experimental systems but rather cause cell death by apoptosis or via the induction of autophagy.

We have previously reported on the anticancer effects and cell death mechanisms of copper imidazo[1,2a]pyridines in five cell lines representing breast and colorectal cancer as well as leukaemia [48]. The active copper complexes decreased cell proliferation with IC₅₀ values in the low micromolar range (< 5 μM) by activating the intrinsic apoptotic pathway [44,49]. The copper complexes modulated the expression of apoptotic inhibitory proteins like XIAP, cIAP-1 and livin, in leukemic and colorectal cancer cell lines, creating a pro-apoptotic environment [44,49]. In addition, we observed an increase in the nuclear expression of haem-oxygenase 1, (HMOX1), an inducible stress response protein implicated in cancer treatment failure [44,49]. An increase in HMOX1 expression in PDAC has been associated with the survival of cancer cells and treatment failure, and its inhibition increased responsiveness to chemotherapy [50]. An increase of HMOX1 expression is required for angiogenesis in pancreatic cancer and cancer of the urinary bladder [51,52]. Currently the role of HMOX1 expression and its induction in cancer remains unresolved, with conflicting data [53].

Due to the limited efficacy of currently used chemotherapy and the

poor outcomes of current treatments, an alternative approach to pancreatic cancer is warranted. In the current study we evaluated the effects of copper complexed to three different types of ligands and their mechanism of cell death on two cell lines representing pancreatic cancer. We investigated further the effect of the copper complexes on HMOX1 expression in the two cell lines and determined the effect of an imidazole-based HMOX1 inhibitor, OB24, on the efficacy of the copper complexes.

2. Materials and methods

2.1. Cell culture

The AsPC-1 and MIA PaCa-2 cell lines were purchased from the ATCC and authenticated using short tandem repeat analysis (Inqaba Biotechnical Industries, South Africa). Cells were grown in sterile conditions in 75 cm² cell culture flasks (Greiner Bio-One, Separations, South Africa) at 37 °C in a 5 % CO₂, humidified incubator. AsPC-1 cells were cultured in Roswell Park Memorial Institute (RPMI) medium obtained from Sigma-Aldrich/Merck (SA) while MIA PaCa-2 cells were grown in a 50/50 (v/v) Dulbecco's Modified Eagle Medium (DMEM) and Ham's F-12 medium (Sigma-Aldrich/Merck, SA). The culture medium was supplemented with 10 % v/v heat-inactivated foetal bovine serum (Gibco, Thermo Fisher, Life Technologies, SA). Cells were routinely checked for mycoplasma contamination using fluorescence microscopy and Hoechst 33342. When cells reached approximately 80 % confluency, they were sub-cultured using standard protocols.

2.2. Test compounds

The copper complexes used in this study were synthesized by the The School of Chemistry, University of the Witwatersrand and the Department of Chemistry at the Nelson Mandela University. The ligands and copper complexes used in this study were solubilized in 100 % cell culture-grade DMSO. The positive control, doxorubicin, was dissolved in 70 % cell-culture grade ethanol (BioUltra, Sigma-Aldrich/Merck, SA). Stock solutions of the compounds were prepared at a concentration of 10 mM. Doxorubicin was selected as a positive control since it was more effective than gemcitabine or cisplatin in the cell culture system.

2.2.1. Synthesis of Cu8AqN and CuPhTh₂

The 8-aminoquinoline-naphthyl copper complex (Cu8AqN) used in this study was synthesized according to the methods described in Myeza et al., 2024 [54]. The phenanthroline-theophylline-copper complex, (CuPhTh₂), was synthesized according to the methods described in Gordon et al., 2022 [55] for complex 3.

2.2.2. Synthesis of the aromatic isoindoline copper complexes

Isoindole ligands were synthesized using a modification of the solventless method used by Addison and Burke (1981) [56]. Phthalonitrile (320 mg, 2.5 mmol), the appropriate amine (5.5 mmol, 2.2 eq) and a catalytic quantity of CaCl₂ were heated together at 175 °C and the reactions were monitored through periodic NMR analysis of the solids until the reactions were complete. This process took between 6 and 24 h. The reaction products were allowed to cool slightly, before the addition of 5 mL of n-Butanol, which was followed by 10 mL water and 2 mL acetonitrile. The insoluble product was filtered and washed with small volumes of water and cold acetonitrile and allowed to air-dry. The structures of the isoindoline ligands were confirmed by NMR.

The isoindoline copper complexes were synthesized using a modified method based on Siegl's work [57]. The ligand (0.33 mmol) and copper acetate dihydrate (0.66 mmol, 2 eq) were added to 5 mL methanol and allowed to stir at room temperature for 48 h. The solvent was removed in vacuo, and the solid product was redissolved in water and filtered to remove unreacted ligand. Following removal of the water, the remaining solid was dissolved in dichloromethane and filtered to remove the

excess copper salt, with the solvent allowed to evaporate slowly. The structures of the isoindoline ligands and their respective copper complexes were confirmed by High Resolution Mass Spectrometry. Mass spectra were recorded with a Bruker compact Q-TOF high resolution mass spectrometer with Bruker Daltonics HyStar 3.2 SR4 software. Chromatograms were analysed with Bruker Compass DataAnalysis software (Version 4.3). The data is presented in the supplementary file, Section S1.

2.3. Cell viability assay

The IC₅₀ values of the copper complexes were obtained from dose-response curves generated from the (3-(4,5-dimethylthiazol-2-yl)-2,5-diphenyltetrazolium bromide) tetrazolium (MTT) assay with modification as described by Dam et al., 2017 [48,58]. Each concentration was tested in quadruplicate and experiments were repeated at least three times. The cells were treated with the copper complexes and positive controls for 48 h. Absorbances of the dissolved formazan crystals were determined using a plate reader at wavelengths of 570 nm and 690 nm and the data was used to determine the percentage of cell survival. The 50 % inhibitory concentration (IC₅₀ value) indicates the potency of a drug or an investigational compound. Sigmoidal dose response curves and IC₅₀ values of the copper complexes were obtained using GraphPad Prism version 9.

Combination experiments using the MTT assay comprised the copper complexes combined with 20 μM of OB24 hydrochloride (OB24), a HMOX1 selective inhibitor, in order to determine the effect of HMOX1-inhibition on the IC₅₀ values of the copper complexes. Student's *t*-test was used to evaluate the statistical significance of the differences in IC₅₀ values obtained from treatment with copper complexes alone compared to IC₅₀ values obtained from treatment with copper complexes and OB24. The significance criterion was set at *p* < 0.05 with a 95 % confidence interval.

2.4. Cell morphology assay

The effects of the copper complexes on the morphology of the cells were assessed after a 24-h treatment with the complexes and doxorubicin. A mixture containing three indicators, Hoechst 33342 (HO) (5 μg/mL) (Sigma-Aldrich/Merck, SA), propidium iodide (PI) (10 μg/mL) (Sigma-Aldrich/Merck, SA) and acridine orange (AO) (10 μg/mL) (Thermo Fisher, Life Technologies, SA) were used to detect morphological changes. Cells were incubated with the dye mixture for 30 min at room temperature, before viewing with the Olympus BX41 epifluorescence microscope. The following filter cubes were used for detection: the U-MNIB3 filter cube for AO (Excitation: 480/20, Emission: 510/50); PI with U-MWIG2 for PI (Excitation: 535/30, Emission: 580 long pass) and the U-MWU2 filter cube for Hoechst 33342 (Excitation: 365/10, Emission 420 long pass). Images were captured with an Olympus DP72 camera (Olympus, Tokyo, Japan). Experiments were repeated three times.

2.5. Annexin-V assay

The Alexa Fluor®-488/Annexin-V Dead Cell Apoptosis Assay (Thermo Fisher, Life Technologies, SA) was used to detect the presence of phosphatidylserine on the cell membrane. Cells were grown on coverslips in six-well plates in 2 mL complete media (per well) and allowed to attach overnight. Cells were then treated with copper complexes and doxorubicin and incubated for 24 h at 37 °C in a 5 % CO₂ atmosphere in a humidified incubator. The annexin-V detection reagent was prepared according to the instructions of the manufacturer. Coverslips were mounted with cells facing downwards onto 50 μL of the reagent mixture on microscope slides. The slides were incubated in the dark in a humidified container at room temperature for 20 min and viewed using an Olympus BX41 epifluorescence microscope. The filter cube U-MNIB3

(Excitation: 480/20, Emission: 510/50) was used to view Alexa Fluor®-488/Annexin-V while filter cube U-MWIG2 (Excitation: 535/30, Emission: 580 long pass) was used to view PI. Images were captured with an Olympus DP72 camera.

2.6. Evaluation of the formation of reactive oxygen species (ROS)

The Invitrogen™ CellRox® Deep Red Reagent (Thermo Fisher, Life Technologies, SA) was used to measure ROS formation. Cells were seeded on glass coverslips in a 6-well plate in 2 mL media per well and allowed to attach overnight at 37 °C in a 5 % CO₂, humidified incubator. The cells were incubated with the copper complexes and doxorubicin before incubation with the CellRox® reagent (2 µL/mL) for 4, 6 and 18 h at 37 °C. A doxorubicin control without CellRox® was included to mitigate the effects of doxorubicin's innate red fluorescence. Following the treatment period, the coverslips were mounted onto microscope slides. Slides were viewed with an Olympus BX41 epifluorescence microscope using the U-MWIG2 filter cube (Excitation: 535/30, Emission: 580 long pass). Images were captured with an Olympus DP72 camera and analysed with the Olympus CellSens Software package.

2.7. Determination of mitochondrial membrane potential (MMP)

The cationic reagent 1,1',3,3'-Tetraethyl-5,5',6,6'-tetrachloroimidacarbocyanine iodide (JC-1) was used to assess the MMP [59]. A decrease in the red/green fluorescence intensity ratio is indicative of mitochondrial depolarisation. Cells were seeded on glass coverslips in six-well plates and allowed to attach overnight at 37 °C in a 5 % CO₂, humidified incubator. Cells were treated with copper complexes and doxorubicin for 18 h. Following washing steps with phosphate buffered saline (PBS), cells were incubated with 500 µL JC-1 reagent (Thermo Fisher, Life Technologies, SA) at a concentration of 1 µL/mL and incubated for 30 min at 37 °C. The coverslips were mounted onto microscope slides and viewed using an Olympus BX41 epifluorescence microscope. The filter cubes used were U-MNIB3 (Excitation: 480/20, Emission: 510/50) and U-MWIG2 (Excitation: 535/30, Emission: 580 long pass). Images were captured with an Olympus DP72 camera and analysed with the Olympus CellSens Software package.

2.8. Measurement of caspase-3/7 activity

Cells were seeded on glass coverslips in six-well plates and allowed to attach overnight at 37 °C in a 5 % CO₂, humidified incubator. Cells were treated with the copper complexes or doxorubicin and incubated for 48 h at 37 °C. Active caspase-3/7 was detected with a 5 µM solution of CellEvent™ Caspase-3/7 Green Detection Reagent prepared in complete media. CellEvent™ Caspase-3/7 Green Detection Reagent was added to each coverslip and incubated for 45 min at 37 °C in the dark. Coverslips were mounted onto microscope slides and viewed with an Olympus BX41 epifluorescence microscope using the U-MNIB3 (Excitation: 480/20, Emission: 510/50) filter cube. Images were captured with an Olympus DP72 camera and analysed with the Olympus CellSens Software package.

2.9. Measurement of caspase-8 activity

Caspase-8 activity was measured in live cells with the Abcam Active Caspase-8 reagent (AB65618). The assay uses a sulfo-rhodamine labelled caspase-8 inhibitor (IETD-FMK) as an in situ detection reagent for active caspase-8. Cells were seeded on sterile glass coverslips in six well plates and incubated overnight to allow for cell attachment to the growth surface. Cells were treated with the copper complexes for 12 h and 24 h at concentrations equivalent to their IC₈₀ values. Doxorubicin was excluded in this assay due to its innate red fluorescence which interfered with the detection of caspase-8 and gave a false positive result. The assay was performed by aspirating the culture media from

the plates and this was followed by two washes with the Abcam proprietary caspase-8 buffer. The caspase-8 detection reagent was prepared in culture media at a dilution of 1 µL per 300 µL. Hoechst-33,342 was added to the mixture to enable the observation of the nuclei. The cells were incubated with the detection reagent of 1 h at 37 °C in a 5 % CO₂, humidified incubator. The reagent was flooded off the coverslips, followed by two gentle wash steps with 2 mL buffer prior to mounting the coverslips on microscope slides. The cells were viewed with an Olympus BX41 epifluorescence microscope at a 400 X magnification, using the appropriate filter cubes and images were captured with an Olympus DP72 camera and processed with the Olympus CellSens software package.

2.10. Measurement of caspase-9 activity

The Caspase-9 (active) FITC Staining Kit (Cat nu ab65615, Abcam) was used to detect active caspase-9. Cells were seeded on glass coverslips in six-well plates and allowed to attach overnight at 37 °C in a 5 % CO₂, humidified incubator. Cells were treated with the copper complexes or doxorubicin and incubated for 24 and 48 h at 37 °C. Following aspiration of the test compounds, cells were washed once with 2 mL PBS. One hundred and fifty microliters of the prepared detection reagent (FITC-LEHD-FMK) was added to each coverslip and incubated for 60 min at 37 °C. Thereafter, cells were washed with PBS and coverslips were mounted onto microscope slides. Slides were viewed using an Olympus BX41 epifluorescence microscope using the U-MNIB3 (Excitation: 480/20, Emission: 510/50) filter cube. Images were captured with an Olympus DP72 camera and analysed with the Olympus CellSens Software package.

2.11. Immunofluorescence detection of HMOX1

Cells were seeded on glass coverslips in a six-well plate and allowed to attach overnight at 37 °C in a 5 % CO₂, humidified incubator. Cells were treated with the copper complexes or doxorubicin for 18 h. Following treatment, cells were fixed by incubating with 3.7 % formaldehyde for 20 min at room temperature. Thereafter cells were permeabilized and non-specific binding was blocked with a solution prepared by combining 100 µL of 25 % Triton X100; 1 mL of 5 % human serum albumin (HSA); and PBS to a final volume of 10 mL. Coverslips were incubated for 10 min at room temperature, before washing with PBS. This was followed by a further blocking step with 0.5 % human serum albumin (HSA) for a further 45 min. Following three washing steps with PBS the cells were incubated overnight with the primary antibody at a 1:200 dilution, which was prepared in 0.5 % HSA. A polyclonal rabbit anti-HMOX1 antibody (PA5-27338) was obtained from Thermo Fisher, Life Technologies, SA). Controls comprised of an untreated negative control and a control incubated only with the secondary antibody.

Following three washing steps with PBS the coverslips were incubated with an appropriate AlexaFluor- 488® conjugated secondary antibody (A32731; Thermo Fisher, Life Technologies, SA) at a 1:800 dilution in 0.5 % HSA for one hour. Following this incubation, the nuclei were counterstained with HO (5 µg/mL) (Sigma-Aldrich/Merck, SA) for 20 min. Coverslips were mounted onto microscope slides using Fluoromount™ (Sigma-Aldrich/Merck, SA) mounting media and allowed to dry before viewing with an Olympus BX41 epifluorescence microscope. The following filter cubes were used: U-MWU2 (Excitation: 365/10, Emission: 420 long pass) for Hoechst 33342; U-MNIB3 (Excitation: 480/20, Emission: 510/50) for HMOX1. Images were captured using an Olympus DP72 camera and analysed with the Olympus CellSens Software package. Experiments were repeated three times.

Fluorescent intensities of the images were measured using CellProfiler™ Image analysis software and is presented as arbitrary values. Ordinary one-way ANOVA followed by Dunnett's post hoc multiple comparisons test was used to evaluate the statistical significance of the

differences of treated cells compared to untreated cells. The significance criterion was set at $p < 0.05$ with a 95 % confidence interval. Colocalisation analysis was done using CellProfiler™ Image analysis software by determining the Pearson's correlation coefficient between the HO signal and the HMOX1 signal.

2.12. Western blotting

Cell lines were treated with the copper complexes or doxorubicin for 18 h. Cell lysates were prepared using RIPA buffer in the presence of a protease inhibitor cocktail tablet (Roche, South Africa). The protein was quantified with the Bradford assay, using the Bio-Rad Protein Assay Kit II (Bio-Rad, SA). Proteins were denatured in Laemmli buffer. The samples containing the same concentration of protein were separated on a discontinuous 12 % SDS-PAGE gel and transferred onto a PVDF membrane. Non-specific binding sites on the membrane were blocked by

incubation in 10 mL Invitrogen™ Membrane Blocking Solution (Thermo Fisher, Life Technologies, SA) for one hour at room temperature. The primary HMOX1 antibody (PA5-27338; (Life Technologies, SA) was prepared at a 1:200 dilution in Invitrogen™ Membrane Blocking Solution (Thermo Fisher, Life Technologies, SA). This was followed by an overnight incubation on a rocking platform at 4 °C and followed by three washing steps with Tris-buffered saline. The membrane was incubated with secondary antibody solution (1:10000) for one hour on a rocking platform at room temperature. The secondary antibody used was Pierce® Goat Anti-Rabbit IgG, (H + L), horseradish peroxidase (HRP) conjugated (#31460, Thermo Fisher, Life Technologies, SA). The bands were detected by chemiluminescence, using the Pierce™ ECL Western Blotting Substrate (Thermo Fisher, Life Technologies, SA) according to the instructions of the manufacturer. The blots were viewed and imaged using the Bio-Rad ChemiDoc™ MP imaging system and analysed using Bio-Rad Image Lab software. Biorad Precision Plus Standards were used

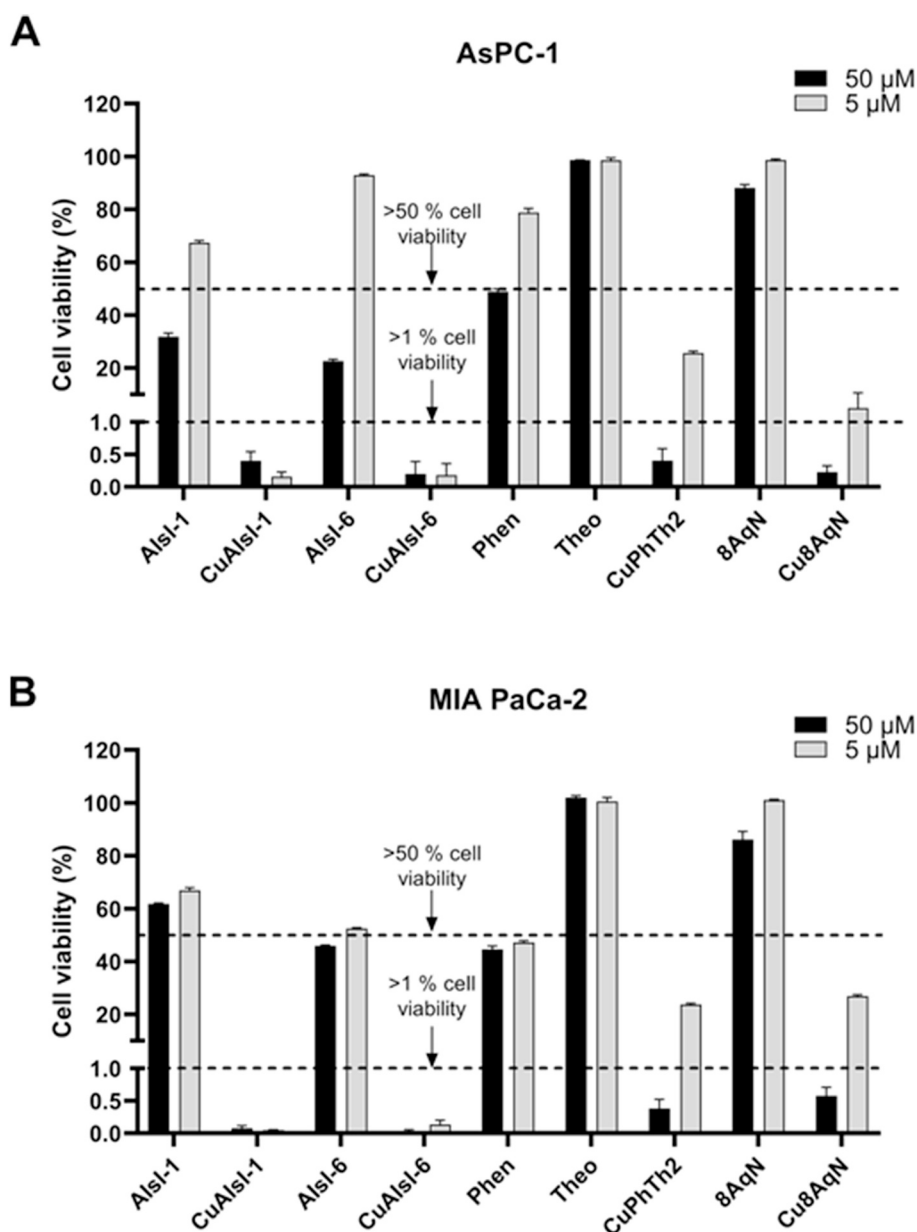


Fig. 1. Copper complexes were more effective inhibitors of AsPC-1 and MIA PaCa-2 cell proliferation than their respective ligands. AsPC-1 cells (A) and MIA PaCa-2 cells (B) were treated with the copper complexes and their respective ligands at concentrations of 50 μM and 5 μM for 48 h. Cell viability was measured with the MTT assay. Each bar represents the mean of four replicate experiments. Error bars represent the standard error of the mean (SEM). (Phen: phenanthroline; Theo: theophylline; 8AqN: ligand of Cu8AqN).

as molecular weight markers.

2.13. Data analysis

Where appropriate, data was analysed using one-way ANOVA followed by Dunnett's post hoc multiple comparison or Student's *t*-test. Significance criterion was set at $p < 0.05$ with a 95 % confidence interval. Graphs indicate the mean \pm SEM and *p*-values are shown where appropriate. All experiments were repeated at least three times and data points were collected in triplicate. Statistical analysis and the construction of graphs were done using GraphPad Prism version 9.

3. Results

3.1. The copper complexes inhibit cell proliferation with low IC₅₀ values

Initial experiments, evaluating the effect of the ligands and their respective copper complexes, confirmed the ability of the copper complexes inhibiting cell proliferation in both pancreatic cancer cell lines as indicated in Fig. 1. The IC₅₀ values, indicating the superior activity of the complexes compared to their respective ligands, and their respective structures are presented in Table 1. The CuAIsI complexes were the most active in both cell lines with IC₅₀ values below 2 μ M. CuPhTh₂ was the least active in both cell lines, although the IC₅₀ value is below 5 μ M. Cu8AqN had IC₅₀ values of 2.75 μ M and 3.62 μ M against AsPC-1 and MIA PaCa-2 cells respectively. Doxorubicin was the least active with IC₅₀ values of 6.64 μ M and 12.07 μ M against AsPC-1 and MIA PaCa-2 cells respectively. All four copper complexes were more effective inhibitors of the Hek-293 cells compared to the pancreatic cancer cells, underscoring the resistance of the pancreatic cancer cells to treatment. Hek-293 cells are used to evaluate the selectivity of investigational compounds for cancer cell lines but are not an absolute indicator for selectivity since it is a transformed cell line. Representative dose response curves are shown in the supplementary document, Fig. S2. Gemcitabine, used in the treatment of pancreatic cancer, requires extensive activation steps and was poorly active in our assay system

after a 48-h treatment period. Therefore, doxorubicin was selected for use as a positive control in the current study.

3.2. In both cell lines, the copper complexes caused apoptotic changes to the nuclei, increased the formation of ROS and increased annexin-V binding

Cell morphology experiments were used to determine the absence or presence of necrotic cell death. These results indicated the absence of necrosis in both cell lines, together with nuclei showing characteristic apoptotic features. Cell membrane blebbing was observed and apoptotic changes to the nuclei included ring and necklace condensation, nuclear fragmentation and chromatin condensation (Fig. 2A and B, green arrows). Cells with red fluorescing nuclei, indicating necrosis, were not detected as shown in Fig. 2. Red/orange lysosomes, detected by AO, were present in the CuAIsI-1, CuAIsI6 and doxorubicin treated AsPC-1 cells, as seen by the presence of punctate perinuclear vesicles (Fig. 2A, yellow arrows). AO is an efficient indicator of acidic compartments within cells [60]. In MIA PaCa-2 cells, (Fig. 2B, pink arrows), the presence of cytoplasmic vacuoles was observed, with the exception of CuAIsI-6 and doxorubicin treated cells.

Since copper complexes are associated with increased ROS formation which cause mitochondrial damage, potentially leading to apoptosis, the effect of the copper complexes on ROS formation was determined. Owing to the short half-lives of ROS [61], the formation of ROS in this study was measured at four-, six- and 18-h treatment periods. The copper complexes caused an increase of ROS formation at 6 h, but not at 4- and 18-h treatment periods. Results are shown in Fig. 3A-D. To compensate for the innate red fluorescence of doxorubicin, a doxorubicin control without the addition of the CellRox reagent was included. This confirmed that doxorubicin caused ROS formation in both cell lines which is consistent with its published mechanism of action [62].

Low levels of ROS were present in untreated AsPC-1 cells, (Fig. 3A, panels a and b and Fig. 4B) which is not uncommon in cancer cells given their high metabolic rate [63]. In AsPC-1 cells, Cu8AqN and doxorubicin caused the greatest increase in fluorescence intensity indicating ROS

Table 1

IC₅₀ values of the four copper complexes and doxorubicin on AsPC-1, MIA PaCa-2 and Hek-293 cells. IC₅₀ values were obtained with the MTT assay after a 48-h treatment period.

Test compound	AsPC-1 cells		MIA PaCa-2 cells		Hek-293 cells	
	IC ₅₀ (μ M)	<i>p</i> -value	IC ₅₀ (μ M)	<i>p</i> -value	IC ₅₀ (μ M)	<i>p</i> -value
CuPhTh ₂	3.15 \pm 0.07	<i>p</i> <0.001	4.04 \pm 0.07	<i>p</i> <0.001	2.1 \pm 0.07	ns
Cu8AqN	2.75 \pm 0.14	<i>p</i> <0.001	3.62 \pm 0.08	<i>p</i> <0.001	1.49 \pm 0.13	<i>p</i> <0.001
CuAIsI-1	1.41 \pm 0.33	<i>p</i> <0.001	1.08 \pm 0.15	<i>p</i> <0.001	0.09 \pm 0.01	<i>p</i> <0.001
CuAIsI-6	1.27 \pm 0.22	<i>p</i> <0.001	1.39 \pm 0.16	<i>p</i> <0.001	0.281 \pm 0.03	<i>p</i> <0.001
Doxorubicin	6.64 \pm 0.11		12.07 \pm 0.61		2.187 \pm 0.033	
Structures of the copper complexes						
<p style="text-align: center;"> CuPhTh₂ Cu8AqN CuAIsI-1 CuAIsI-6 </p>						

The IC₅₀ values of the copper complexes were compared with doxorubicin by ANOVA, followed by Dunnett's post hoc test. The significance criterion was set at $p < 0.05$.

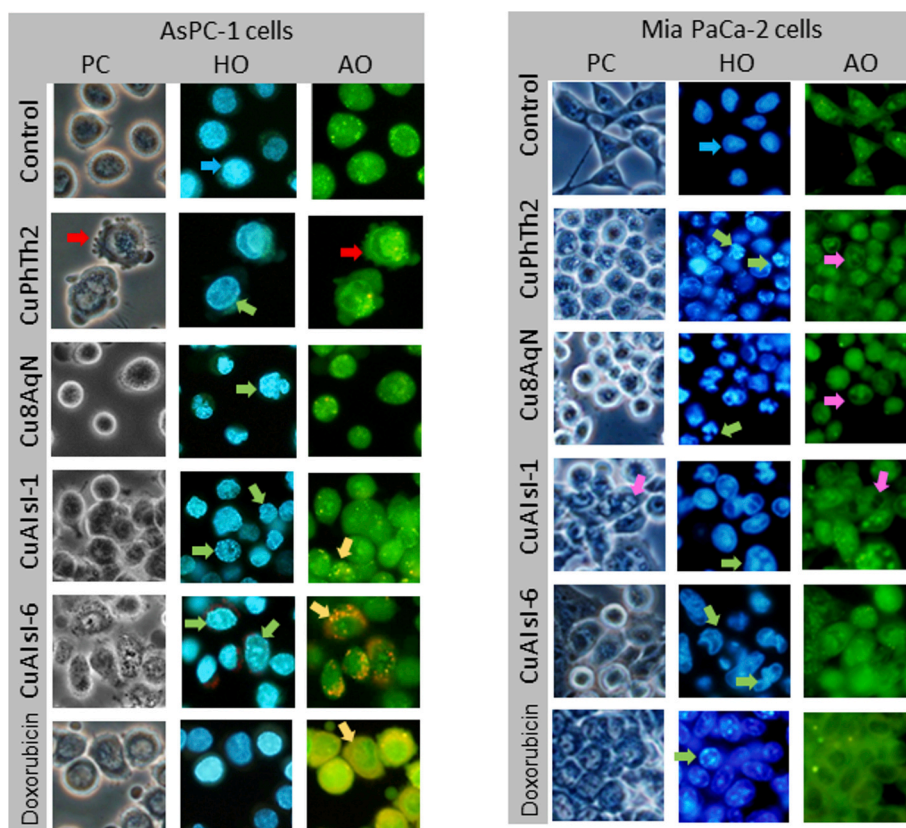


Fig. 2. Representative photomicrographs showing morphological changes in AsPC-1 and MIA PaCa-2 cells after a 24-h treatment with copper complexes. AsPC-1 cells (A) were treated with 6 μM CuPhTh₂, 4 μM Cu8AqN, 2 μM CuAISI-1, 2 μM CuAISI-6 and 5 μM doxorubicin for 24 h. MIA PaCa-2 cells (B) were treated with 6 μM CuPhTh₂, 5 μM Cu8AqN, 2 μM CuAISI-1, 2 μM CuAISI-6 and 5 μM doxorubicin for 24 h. Cells were viewed with an Olympus BX41 microscope and images were captured with an Olympus DP72 camera. Magnification: 400 \times . Each photomicrograph is representative of three independent experiments. PC: phase contrast, HO: Hoechst 33342, AO: acridine orange. Arrow legend: Red: membrane blebbing, Blue: normal nuclei, Green: apoptotic nuclei, Yellow: lysosomes, Pink: vacuoles. (For interpretation of the references to colour in this figure legend, the reader is referred to the web version of this article.)

formation (Fig. 3A panels e, f, k, l and Fig. 3B), followed by CuPhTh₂, CuAISI-1 and CuAISI-6 (Fig. 3A panels c, d, g, h, i, j and Fig. 3B). In MIA PaCa-2 cells ROS was not observed in the untreated control cells (Fig. 3C panels a and b) whilst all four copper complexes caused a significant increase in ROS (Fig. 3C panels c-j and Fig. 3D) albeit significantly less than that caused by doxorubicin (Fig. 3C panels k and i). ROS formation was more pronounced in MIA PaCa-2 than in AsPC-1, when comparing Fig. 3B and D. Doxorubicin was significantly more effective than the copper complexes at inducing the formation of ROS in both cell lines, at the time periods tested (Fig. 3B and D).

The annexin-V binding assay was used to determine the presence of phosphatidyl serine on the outer plasma membrane and to confirm apoptotic cell death. Results from this assay are shown in Fig. 3E, F, G and H. In AsPC-1 cells the four complexes significantly increased annexin-V binding indicating an increase in phosphatidylserine on the outer leaflet of the cell membrane, an early marker of apoptosis (Fig. 3E, panels c-j and Fig. 3F). In MIA PaCa-2 cells both early and late apoptotic cells were seen, as indicated by the red-fluorescing nuclei in combination with the green annexin-V fluorescing cell membranes (Fig. 3H, panels c-j and Fig. 3D). This is indicative of possible secondary necrosis which commonly occurs in cell culture assays since there is no mechanism for removing apoptotic cells from cell cultures. As seen in Fig. 3F in AsPC-1 cells, the copper complexes were less effective than doxorubicin as inducers of phosphatidylserine localisation to the outer cell membrane. The four copper complexes caused membrane blebbing in AsPC-1 cells (Fig. 3E, panels c, e and g). In MIA PaCa-2 cells (Fig. 3G), CuAISI-6 shows a greater percentage of cells positive for annexin-V binding than doxorubicin. The other copper complexes were similar to doxorubicin as

inducers of annexin-V binding.

3.3. The copper complexes activated the intrinsic apoptotic pathway by decreasing mitochondrial membrane potential (MMP) and activating caspase-9 whilst failing to cause the early activation of caspase-8

3.3.1. The copper complexes caused a loss of MMP

The four copper complexes and doxorubicin caused the near complete loss of MMP in both cell lines as indicated by the predominant green fluorescence observed in the treated cells (Fig. 4A-D). In AsPC-1 cells the control cells showed yellow and orange/red fluorescence indicating an intact MMP (Fig. 4A, panel a and Fig. 4B). Red and orange fluorescence was absent in all the treated cells (Fig. 4A panels b – f, and Fig. 4B). The granular appearance of the green fluorescence indicates structurally intact mitochondria whilst an even green fluorescence suggests the loss of mitochondrial structural integrity. This was the primary observation in AsPC-1 cells treated with CuAISI-6 and doxorubicin (Fig. 4A, panels e and f). The other copper complexes caused a mixture of cells displaying either granulated or an even green fluorescence.

In a similar fashion, in MIA PaCa-2 cells, there was a complete loss of MMP, as indicated in Fig. 4C panels b – e, when compared with Fig. 4C, panel a. All the complexes caused a loss of the punctate fluorescence observed in the untreated cells (Fig. 4C, panel a). In doxorubicin-treated MIA PaCa-2 cells the green fluorescence dominates with some red fluorescence present in the nuclei, indicative of doxorubicin's nuclear localisation.

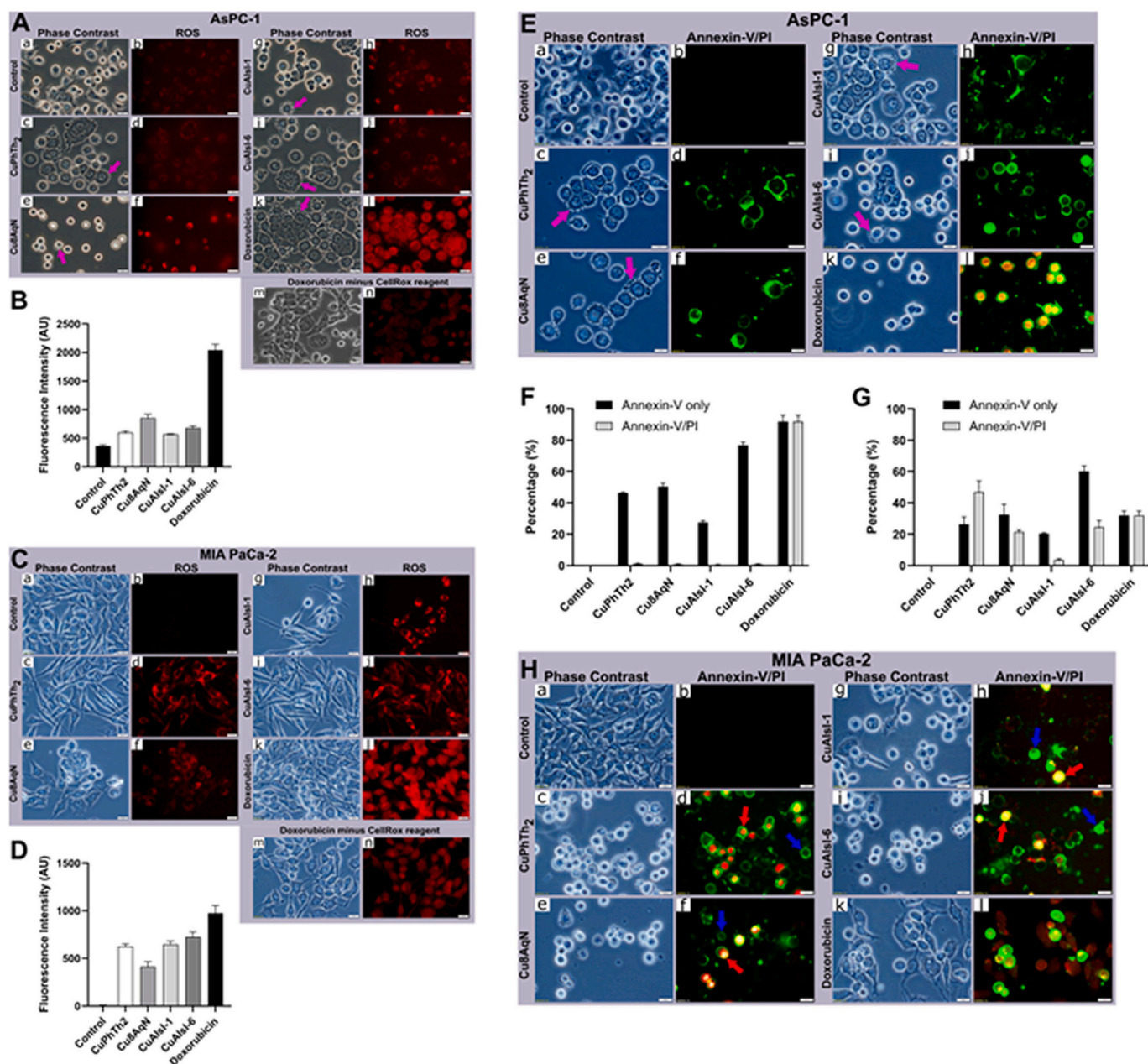


Fig. 3. The copper complexes increased ROS formation and the binding of annexin-V to phosphatidylserine in AsPC-1 and Mia PaCa-2 pancreatic cancer cell lines. Parts A, B, C and D represents the effects of copper complexes on ROS formation after a 6 h treatment period. A and C are representative photomicrographs with the red fluorescence indicating ROS and C and D represents the fluorescence intensity observed from three independent experiments. Parts E and H are representative photomicrographs of annexin-V binding with green fluorescence indicating annexin-V binding and red fluorescence indicating PI staining of nuclei. F and G are bar graphs showing the percentage cells positive for annexin-V after a 24 h treatment with copper complexes. Cells were treated as follows; CuPhTh₂ (6 μ M), Cu8AqN (4 μ M for AsPC1 and 5 μ M for MIA PaCa-2 cells respectively), CuAISI-1 (2 μ M), CuAISI-6 (2 μ M), and doxorubicin (5 μ M). Cells were viewed with an Olympus BX41 microscope and images captured with an Olympus DP72 camera. Magnification: 400 x, scale bar: 20 μ m. Each photomicrograph is representative of three independent experiments. Each bar represents the mean and SEM of three independent experiments. Pink arrows: membrane blebbing, red arrows: late apoptosis, blue arrows: early apoptosis. (For interpretation of the references to colour in this figure legend, the reader is referred to the web version of this article.)

3.3.2. The copper complexes activated caspase-9

Mitochondrial membrane depolarisation is associated with the activation of the intrinsic apoptotic pathway which depends on the formation of the apoptosome which contains active caspase-9. Active caspase-9 was present in both cell lines following treatment with the copper complexes as seen in Fig. 5A-D. In AsPC-1 cells CuPhTh₂ was the weakest caspase-9 activator with the lowest percentage of cells (~ 50 %) showing active caspase-9 (Fig. 5A, panels c and d and Fig. 5B). Caspase-9 activity in the other copper complexes compared well to that of doxorubicin with no significant differences observed (Fig. 5A panels e-j and

Fig. 5B). In MIA PaCa-2 cells, the aromatic isoindoline copper complex, CuAISI-6 had the lowest percentage of cells with active caspase-9 (Fig. 5C panels i and j and Fig. 5D). The other three copper complexes increased caspase-9 activity to between 70 % and 90 %, similarly to doxorubicin (Fig. 5C, panels c-h and Fig. 5D). The increase in caspase-9 activity observed in both cell lines by the four copper complexes indicated that apoptosis was facilitated by the activation of the intrinsic apoptotic pathway.

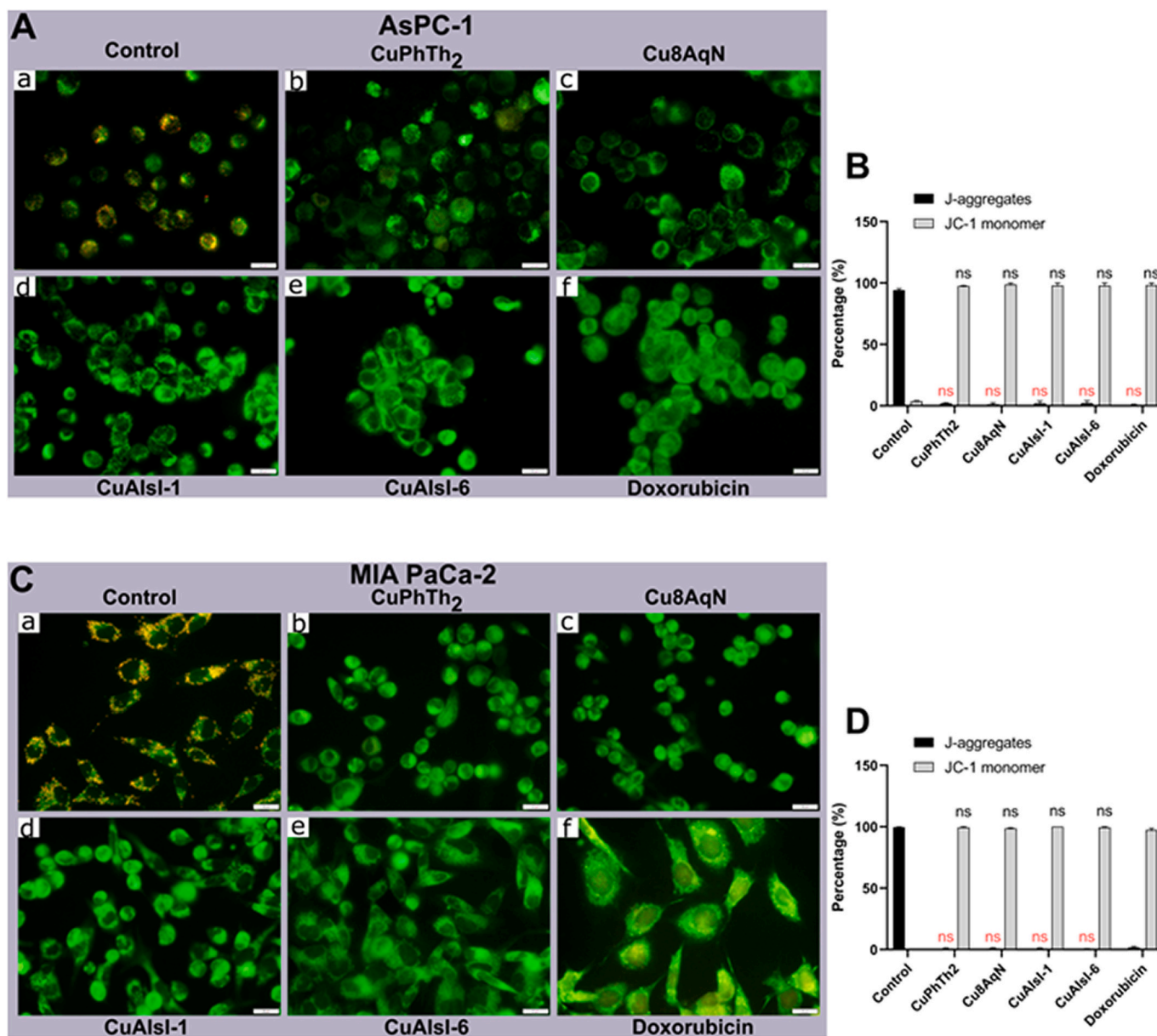


Fig. 4. Copper complexes decreased the MMP in ASPC-1 and MIA PaCa-2 cells. Photomicrographs in 4 A and 4C shows images of red JC-1-aggregates and green JC-1 monomers and 4B and 4D shows the percentage of cells with JC aggregates and monomers of three experiments. Effects of the copper complexes on ASPC1 cells are shown in 4 A and 4B and on Mia PaCa-2 cells in 4C and D. Cells were treated as follows; CuPhTh₂ (6 μ M), Cu8AqN (4 μ M for ASPC1 and 5 μ M for MIA PaCa-2 cells respectively), CuAIsI-1 (2 μ M), CuAIsI-6 (2 μ M), and doxorubicin (5 μ M). Cells were viewed with an Olympus BX41 microscope and images captured with an Olympus DP72 camera. Magnification: 400 x, scale bar: 20 μ m. Each photomicrograph is representative of three independent experiments and each bar graph represents the mean from three independent experiments, with error bars representing the SEM. Copper complexes were compared to doxorubicin using ANOVA ($p < 0.05$) followed by Dunnett's post hoc multiple comparisons test. (For interpretation of the references to colour in this figure legend, the reader is referred to the web version of this article.)

3.3.3. The copper complexes failed to induce the early activation of caspase-8

Activation of caspase-8 is an early indicator for the activation of death receptors and the subsequent activation of the extrinsic apoptotic pathway. We could not demonstrate meaningful activation of caspase-8 in both cell lines during the first 24 h following the start of treatment. We did however observe that cells with signs of advanced deterioration were positive for caspase-8. The caspase-8 data is presented in the supplementary file, Section S3, Figs. S2 and S3 for ASPC-1 and Mia PaCa-2 cells respectively.

3.4. The copper complexes activate caspase-3/7 in both cell lines

Further to the activation of caspase-9, their ability of the copper complexes to activate caspase-3/7 in the two cell lines was evaluated. After treatment with the copper complexes, active caspase-3/7 was observed in both cell lines as shown in Fig. 6A-D. Cu8AqN was the most efficient activator of caspase-3/7 in ASPC-1 cells (Fig. 6A panels e, f and Fig. 6B), while CuAIsI-1 was the poorest activator at this treatment period with a low percentage of cells with active caspase-3/7 (Fig. 6A panels g, h and Fig. 6B). CuPhTh₂ and CuAIsI-6 was moderately active with around 30 % of cells with active caspase-3/7 (Fig. 6A, panels c, d, i, j and Fig. 6B). All the copper complexes were less efficient than doxorubicin which had close to 90 % of cells with active caspase-3/7 (Fig. 6A

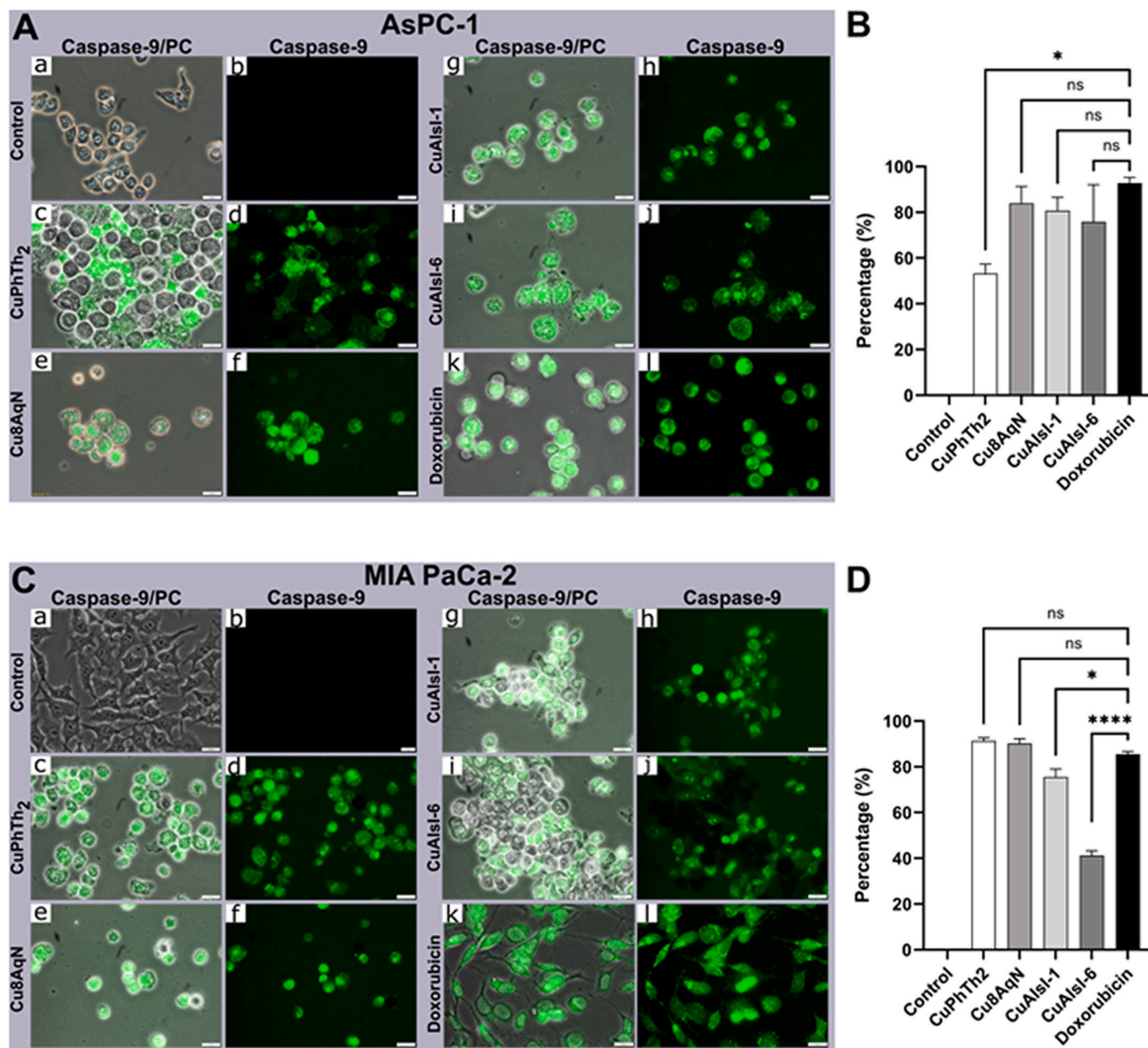


Fig. 5. The copper complexes caused an increase in active caspase-9 in AsPC-1 and MIA PaCa-2 cells. Photomicrographs in 5A and 5C show the presence of active caspase-9, visible as green fluorescence, and 5B and 5D show the average percentage of cells with active caspase-9 from three independent experiments. The effect of the copper complexes on AsPC-1 cells is shown in 5A and 5B and the effect on MIA PaCa-2 cells is shown in 5C and 5D. Cells were treated as follows; panel a: untreated cells, panel b: CuPhTh₂ (6 μ M) panel c: Cu8AqN (4 μ M for AsPC-1 and 5 μ M for MIA PaCa-2 cells respectively), panel d: CuAlsl-1 (2 μ M), panel e: CuAlsl-6 (2 μ M), panel f: doxorubicin (5 μ M). Cells were viewed with an Olympus BX41 microscope and images were captured with an Olympus DP72 camera. Magnification: 400 \times , scale bar: 20 μ m. Each photomicrograph is representative of three independent experiments and each bar represents the mean from three independent experiments. Error bars represent SEM. The effect of the copper complexes was compared to doxorubicin using ANOVA ($p < 0.05$) followed by Dunnett's post hoc multiple comparison test. (For interpretation of the references to colour in this figure legend, the reader is referred to the web version of this article.)

panels k, l, and Fig. 6B).

In comparison, in MIA PaCa-2 cells all the copper complexes and doxorubicin proved to be efficient activators of caspase-3/7 with close to 100 % of cells positive for caspase-3/7 (Fig. 6C and D). All the complexes showed similar or better caspase-3/7 activity than doxorubicin (Fig. 6C panels c-l), indicating their ability to activate the intrinsic apoptotic pathway in MIA PaCa-2 cells.

3.5. Copper complexes induced HMOX1 expression in AsPC-1 and MIA PaCa-2 cells and its inhibition increased the potency of the copper complexes

3.5.1. Copper complexes increased the nuclear expression of HMOX1

Expression levels of HMOX1 was determined by immunofluorescence microscopy and western blotting. In AsPC-1 cells no fluorescence was present in the untreated primary antibody-negative control, indicating the specificity of the primary antibody (Fig. 7A panels a-c). Baseline HMOX1 expression was observed in the nuclei of untreated AsPC-1 cells (Fig. 7A panels d-f). There was a visible increase in fluorescence intensity of HMOX1 in all treated cells, compared to untreated

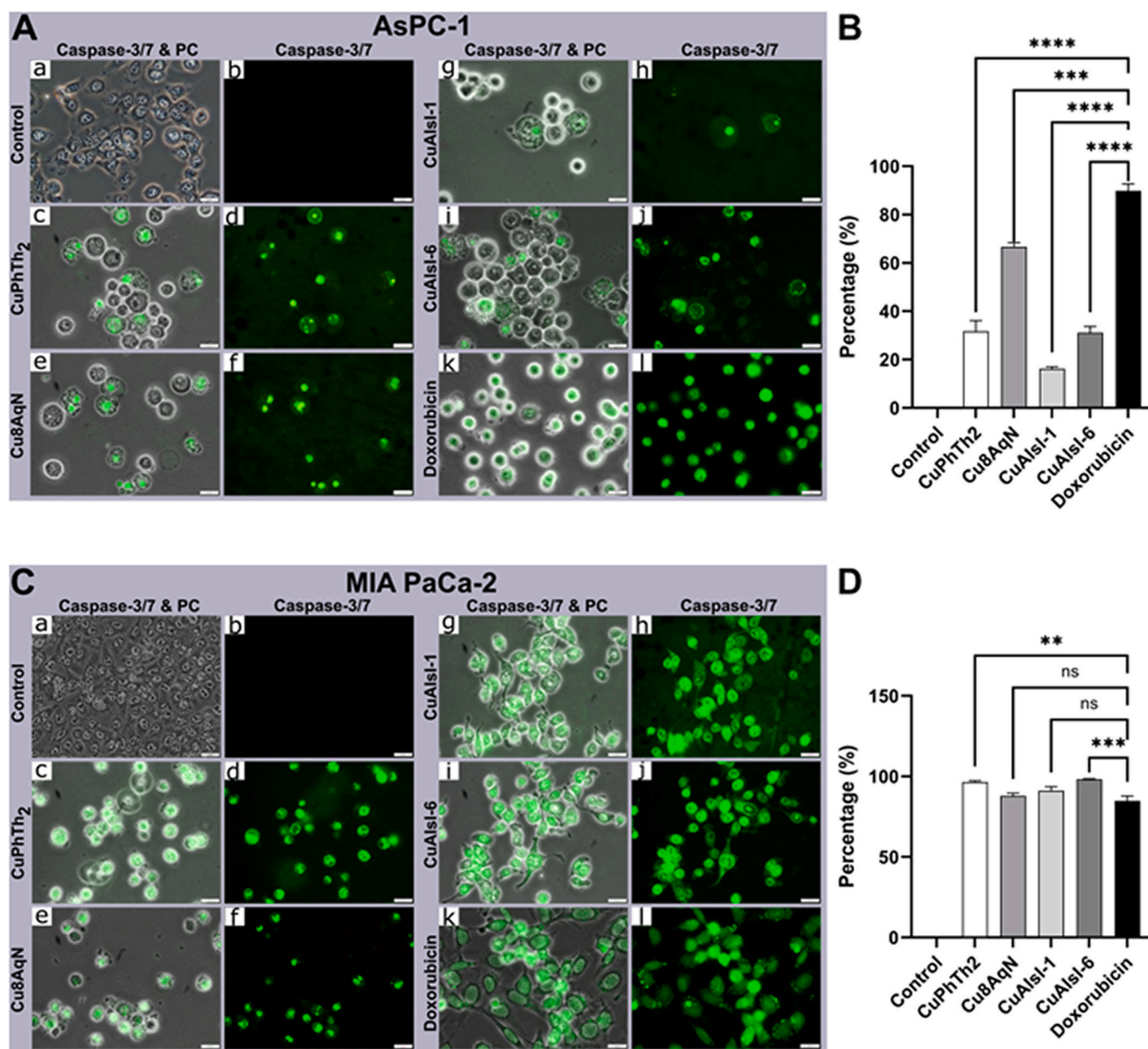


Fig. 6. The copper complexes activated caspase-3/7 in ASPC-1 and MIA PaCa-2 cells. Photomicrographs in 6A and 6C shows the presence of active caspase-3/7 visible as green fluorescence and 6B and 6D shows the average percentage of cells with active caspase-3/7 from three independent experiments. The effect of the copper complexes on ASPC-1 cells is shown in 6A and 6B and the effect on MIA PaCa-2 cells is shown in 6C and 6D. Cells were treated as follows; panel a: untreated cells, panel b: CuPhTh₂ (6 μ M), panel c: Cu8AqN (4 μ M for ASPC-1 and 5 μ M for MIA PaCa-2 cells respectively), panel d: CuAISI-1 (2 μ M), panel e: CuAISI-6 (2 μ M), panel f: doxorubicin (5 μ M). Cells were viewed with an Olympus BX41 microscope and images were captured with an Olympus DP72 camera. Magnification: 400 \times , scale bar: 20 μ m. Each photomicrograph is representative of three independent experiments. Each bar represents the mean from three independent experiments and error bars represent the SEM. The effect of the copper complexes was compared with doxorubicin using ANOVA ($p < 0.05$) followed by Dunnett's post hoc multiple comparisons test. (For interpretation of the references to colour in this figure legend, the reader is referred to the web version of this article.)

cells (Fig. 7A panels g-u), indicating that the copper complexes and doxorubicin induced the expression of HMOX1. Fluorescence intensity analysis showed CuPhTh₂ to be the strongest inducer of HMOX1 while Cu8AqN was the weakest (Table 2). Compared with the copper complexes, doxorubicin had the second highest fluorescence intensity measurement. Colocalisation analysis using Pearson's correlation coefficient (PCC) between Hoechst and HMOX1 fluorescence was used to quantify changes in the subcellular location of HMOX1. The analysis indicated that HMOX1 was located primarily in the nucleus, following treatment with the copper complexes (Table 2). Conversely, in doxorubicin treated cells, the percentage of HMOX1 in the nucleus was decreased when compared to the untreated cells (Table 2).

In MIA PaCa-2 cells the absence of green fluorescence in the untreated primary antibody-negative control of MIA PaCa-2 cells indicated the specificity of the primary antibody for HMOX1 (Fig. 7B, panels a-c). Untreated MIA PaCa-2 cells had low levels of basal HMOX1 expression (Fig. 7B, panels d-f). The copper complexes and doxorubicin increased the expression of HMOX1, indicated by the increased intensity and numbers of green fluorescing cells, compared with the untreated control (Fig. 7B, panels g-u). Fluorescence intensity analysis showed CuPhTh₂ to be the strongest HMOX1 inducer, similar to the ASPC-1 cells, while CuAISI-6 was the weakest inducer (Table 2). Doxorubicin had the smallest increase in fluorescence intensity, suggesting that the copper complexes induced HMOX1 more potently than doxorubicin (Table 2).

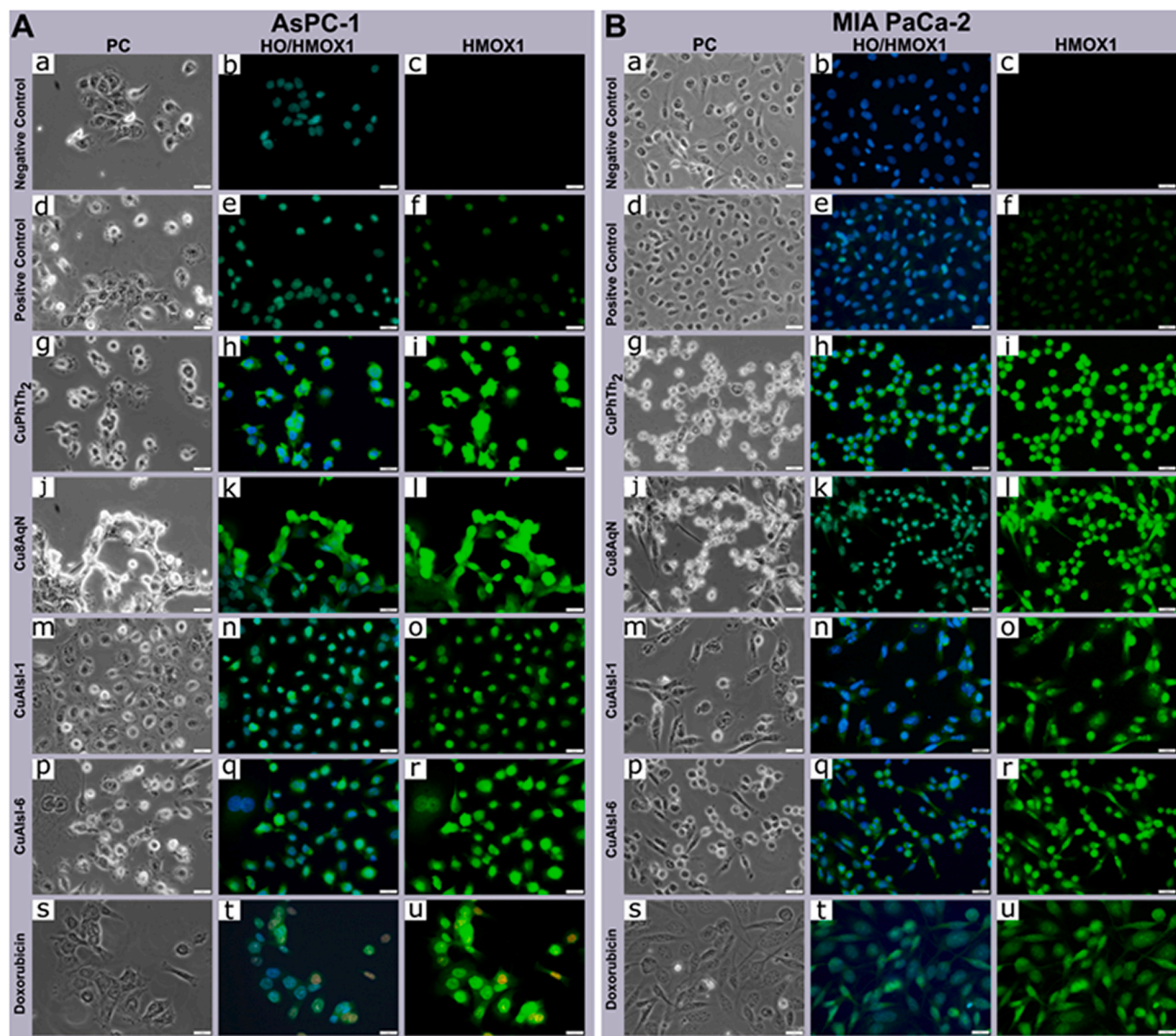


Fig. 7. Representative photomicrographs showing the induction of HMOX1 expression by the copper complexes and doxorubicin in AsPC-1 and Mia PaCa-2 cells. Green fluorescence indicates the presence and intensity of HMOX1 and blue fluorescence indicates the nuclei. An untreated negative control without primary antibody (panels a-c) and an untreated positive control with primary antibody (panels d-f) was included. AsPC1 cells (A) were treated with CuPhTh₂ at 6 μ M (g-i); Cu8AqN at 4 μ M (j-l); CuAIsI-1 at 2 μ M (m-o) and CuAIsI-6 at 2 μ M (p-r) for 18 h. Doxorubicin was used as a positive control at 5 μ M (panels s-u). Mia PaCa-2 cells (B) were treated with CuPhTh₂ at 6 μ M (g-i); Cu-8AqN at 5 μ M (j-l); CuAIsI-1 at 2 μ M (m-o) and CuAIsI-6 at 2 μ M (p-r) for 18 h. Doxorubicin was used as a positive control at 5 μ M (panels s-u). Cells were viewed with an Olympus BX41 microscope and images were captured with an Olympus DP72 camera. Legend: PC = Phase contrast. HO = Hoechst 33342. HMOX1 = haem oxygenase-1. Magnification: 400 \times , scale bar: 20 μ m. Each photomicrograph is representative of three independent experiments. (For interpretation of the references to colour in this figure legend, the reader is referred to the web version of this article.)

Colocalisation analysis indicated that HMOX1 was primarily localized to the nucleus of the cells treated with the copper complexes as verified by an increase in PCC between HO and HMOX1 (Table 2). The exception was in doxorubicin-treated cells where the largest fraction of HMOX1 was located in the cytoplasm (Table 2).

3.5.2. Western blotting confirmed the increase of HMOX1 expression

Cell lysates were prepared from treated AsPC-1 and Mia PaCa-2 cells and were used to confirm the results of the HMOX immunofluorescence by western blotting (Fig. 8). Analysis of the western blots indicated that CuPhTh₂ was the most potent inducer of HMOX1 in both cell lines which was consistent with the immunofluorescence observations (Fig. 8A-D). In AsPC-1 cells, Cu8AqN, CuAIsI-1 and CuAIsI-6 caused similar increases

of HMOX1, which was lower than that of CuPhTh₂. In doxorubicin treated cells, no bands were detected.

In Mia PaCa-2 cells, Cu8AqN caused a larger increase than CuAIsI-1 and CuAIsI-6 but lower than CuPhTh₂ (Fig. 8B and D). CuAIsI-1 was the weakest inducer of HMOX1 in Mia PaCa-2 cells. A faint band was present in doxorubicin treated cells, indicating that HMOX1 expression was not increased. Analysis of the molecular weight indicated that the size of HMOX1 was 32 kDa, for both cell lines, suggesting a full-length HMOX1 protein.

3.5.3. The HMOX1 inhibitor, OB24, decreased the IC₅₀ values of the copper complexes

Next, the effects of an HMOX1 inhibitor on the potency of the four

Table 2

The mean fluorescence intensity and nuclear localization of HMOX1 in AsPC-1 and MIA PaCa-2 cells following treatment with the copper complexes and doxorubicin for 18 h.

AsPC-1 cells				
Test Compound	Mean Fluorescence Intensity (AU)	p-value	Nuclear localization (PCC)	% Nuclear localization
Control	295.5 ± 15.04		0.767 ± 0.030	76.7
CuPhTh ₂	1082.0 ± 34.1	p = <0.001	0.816 ± 0.013	81.6
Cu-8AqN	747.5 ± 36.8	p = <0.001	0.878 ± 0.016	87.8
CuAISI-1	881.6 ± 38.7	p = 0.0015	0.867 ± 0.003	86.7
CuAISI-6	848.8 ± 7.1	p = <0.001	0.843 ± 0.017	84.3
Doxorubicin	1046 ± 18.5	p = <0.001	0.578 ± 0.004	57.8
MIA PaCa-2 cells				
Test Compound	Mean Fluorescence Intensity (AU)	p-value	Nuclear localization (PCC)	Nuclear localization (%)
Control	173.1 ± 7.6		0.721 ± 0.043	72.1
CuPhTh ₂	908.4 ± 36.8	p = <0.001	0.899 ± 0.021	89.9
Cu-8AqN	733.4 ± 8.8	p = <0.001	0.879 ± 0.004	87.9
CuAISI-1	661.7 ± 12.7	p = <0.001	0.888 ± 0.012	88.8
CuAISI-6	558.2 ± 17.9	p = <0.001	0.869 ± 0.010	86.9
Doxorubicin	360.1 ± 13.3	p = <0.001	0.590 ± 0.014	59.0

The fluorescence intensity of treated cells was compared with that of untreated cells using ANOVA followed by Dunnett's post hoc test. $P > 0.05$: not significant (ns), AU: arbitrary units, PCC: Pearson's correlation coefficient.

copper complexes were investigated. The IC₅₀ values of the copper complexes on AsPC-1 and MIA PaCa-2 cells were determined in the presence of a constant concentration of a HMOX1 selective inhibitor 1-[[2-[2-(4-Bromophenyl)ethyl]-1,3-dioxolan-2-yl]methyl]-1H-imidazole.HCl, commonly referred to as OB24. OB24 is reported to inhibit HMOX1 selectively with an IC₅₀ of 1.9 μM and is not active against HMOX2 with an IC₅₀ value exceeding 100 μM [64]. At the concentrations tested, (10 μM, 20 μM and 40 μM), OB24 by itself showed no meaningful cytotoxic effects, therefore the Chou-Talalay method was not used to determine synergy or antagonism. In this study OB24 was used a concentration of 20 μM.

The decreases in the IC₅₀ values of the copper complexes obtained in the presence of OB24 are shown in Table 3 and were statistically significant. Given that OB24 did not display cytotoxic activity against the cell lines on its own, it can be concluded that the observed decreases were not due to the cytotoxic activity of OB24, but rather to its inhibition of HMOX1. The results indicate that HMOX1 inhibition sensitized the pancreatic cancer cell lines to the copper complexes.

4. Discussion

4.1. The copper complexes inhibited cell growth with clinically relevant IC₅₀ values which were further decreased by a HMOX1 inhibitor

The IC₅₀ values of the four copper complexes were in the low micromolar range for both PDAC cell lines, with the two aromatic isoindoline copper complexes being the most active. The respective ligands of the four complexes were poorly active at 5 μM, indicating that the addition of copper to the ligands enhanced their cytotoxic activity. The phenanthroline-theophylline based copper complex, CuPhTh₂, was the least active in the two cell lines. All four complexes had IC₅₀ values below 5 μM after a 48-h treatment, while doxorubicin was less active in both cell lines with IC₅₀ values above 6 μM. In this study, we chose to use

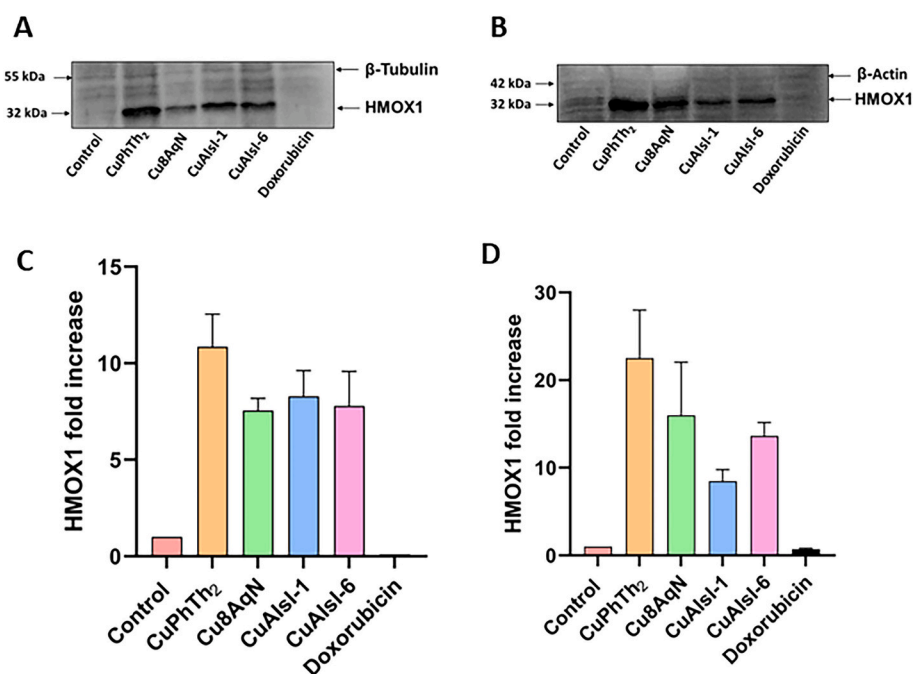


Fig. 8. Western blots and bar graphs showing the expression level of HMOX1 in AsPC-1 (A and C) and MIA PaCa-2 cells (B and D). AsPC-1 cells were treated with copper complexes and doxorubicin at the following concentrations: CuPhTh₂ at 6 μM; Cu8AqN at 4 μM; CuAISI-1 at 2 μM and CuAISI-6 at 2 μM and doxorubicin at 5 μM for 18 h. MIA PaCa-2 cells were treated with copper complexes at the following concentrations: CuPhTh₂ at 6 μM; Cu8AqN at 5 μM; CuAISI-1 at 2 μM and CuAISI-6 at 2 μM and doxorubicin at 5 μM for 18 h. Lysate samples containing 20 μg protein were separated using a 12 % denaturing polyacrylamide gel. β-tubulin was used as a loading control in AsPC-1 cells and in MIA PaCa-2 cells β-actin was used. Chemiluminescent bands were detected with a Bio-Rad ChemiDoc™ MP Imaging system and the blots were analysed using Bio-Rad Image Lab software. A and B are representative western blot images of AsPC-1 and MIA PaCa-2 cells respectively. C and D represents the average fold increase of HMOX1 of three independent experiments of AsPC-1 and MIA PaCa-2 cells respectively. Error bars represent the SEM.

Table 3

The IC₅₀ values of copper complexes alone and in combination with 20 μM of a HMOX1 inhibitor, OB24, in AsPC-1 and MIA PaCa-2 cells.

AsPC-1 cells			
Copper complex	IC ₅₀ value (μM) without OB24	IC ₅₀ value (μM) with 20 μM OB24	p-value
CuPhTh ₂	3.15 ± 0.07 μM	2.79 ± 0.04 μM	p = 0.0108
Cu8AqN	2.75 ± 0.14 μM	1.01 ± 0.10 μM	p < 0.0001
CuAIsI-1	1.41 ± 0.33 μM	0.18 ± 0.03 μM	p = 0.0216
CuAIsI-6	1.27 ± 0.22 μM	0.19 ± 0.04 μM	p = 0.0022
MIA PaCa-2 cells			
Copper complex	IC ₅₀ value (μM) without OB24	IC ₅₀ value (μM) with 20 μM OB24	p-value
CuPhTh ₂	4.04 ± 0.07 μM	1.83 ± 0.15 μM	p < 0.0001
Cu8AqN	3.62 ± 0.08 μM	2.45 ± 0.07 μM	p < 0.0001
CuAIsI-1	1.08 ± 0.15 μM	0.59 ± 0.05 μM	p = 0.0404
CuAIsI-6	1.39 ± 0.16 μM	0.77 ± 0.16 μM	p = 0.0363

Student's *t*-test was used to compare the IC₅₀ values of copper complexes with and without OB24 with a significance criterion set at $p \leq 0.05$.

doxorubicin as a positive control rather than gemcitabine. Our data (not shown) indicated that the IC₅₀ values of gemcitabine were greater than 200 μM in both cell lines, suggesting either an inability of gemcitabine to enter the cells or a failure to activate the molecule to its active triphosphate form. The copper complexes were evaluated for cytotoxicity after 48-h treatment periods rather than the commonly published 72 h. A 72-h treatment in cell culture has the caveat that rapidly dividing cells deplete the culture medium, making them more susceptible to test compounds, thereby causing an overestimation of the compounds' potency. The IC₅₀ values for the HEK-293 embryonic kidney cell line were markedly lower than those for the PDAC cancer cell lines, aligning with PDAC's well-documented resistance to chemotherapy. This highlights the importance of considering potential adverse reactions in future studies with these copper complexes. Moreover, evaluation of a single cell line does not provide conclusive data to exclude these copper complexes from further investigation. Many cancer drugs currently in clinical use are known for specific toxicity, with established protocols in place to mitigate associated adverse events effectively. Follow-up investigations aimed at understanding the mechanism of cell death, used concentrations equivalent to the IC₈₀ values of the copper complexes since clinically, cancer is treated with concentrations of drugs aiming to get a 100 % cell kill, rather than a 50 % cell kill. The aromatic isoindoline-based copper complexes were significantly more active than the 8-aminoquinoline-naphthyl and the phenanthroline-theophylline copper complexes. Importantly, the IC₅₀ values of all four complexes, in both cell lines, were significantly reduced in the presence of an imidazole-based HMOX1 inhibitor, supporting those studies indicating that induced HMOX1 expression is associated with treatment failure in pancreatic cancer [50–53]. In order to study the events responsible for cell death we determined the effects of the copper complexes on cell death parameters at treatment periods shorter than 48 h, where applicable.

4.2. The copper complexes caused cell death by activation of the intrinsic apoptotic pathway

Once the potency of the copper complexes was established it was important to rule out necrosis as the primary mechanism of cell death. Evaluation using a live cell assay indicated that none of the four complexes showed any evidence of causing necrotic cell death, as seen by the absence of red-fluorescing nuclei, indicating intact cell membranes.

Membrane blebbing was observed in some instances, further supporting the notion of apoptotic cell death. Changes to the nuclei included ring and necklace condensation, fragmentation and chromatin condensation (all features of apoptosis), and were observed for all the treated cells [65,66].

Following the promising IC₅₀ values and the absence of necrosis in the treated cells, we further investigated the ability of the copper complexes to cause apoptotic cell death. In both cell lines, the complexes increased the translocation of phosphatidylserine, as seen with increased binding of AlexaFluor-488 labelled annexin-V, which further supported apoptotic cell death. Annexin-V assays however did indicate the presence of late apoptotic MIA PaCa-2 cells, positive for both annexin-V and PI, which is considered to be secondary necrosis, often observed in cultured cell lines [67]. In both cell lines, CuAIsI-6 was the most effective inducer of annexin-V whilst CuAIsI-1 was the least effective. Doxorubicin was more effective in AsPC-1 cells, with 95 % of the cells showing annexin-V-binding compared with the 31 % in MIA PaCa-2 cells.

The ability of other copper complexes to cause annexin-V binding is widely reported in the literature. Copper-imidazo[1,2-*a*]pyridines induced annexin-V binding in leukemic cell lines [41] as well as in colorectal cancer cell lines [40]. Additionally, polypyridyl based copper (II) complexes increased annexin-V binding in breast cancer cells [68]. Ternary copper (II) complexes with reduced Schiff base ligands and heterocyclic bases, which also included a phenanthroline-based copper complex, were able to induce annexin-V binding in human lung, oesophageal and gastric cancer cell lines [69].

Copper complexes are associated with the formation of ROS, which interact with DNA, causing DNA damage and the formation of oncogenic mutations that drive tumorigenesis [70,71]. In both cell lines doxorubicin was the most potent inducer of ROS which is consistent with its mechanism of action [62]. Untreated AsPC-1 cells had low baseline ROS levels, unlike MIA-Paca 2 cells where ROS was not detected. All the copper complexes increased ROS, albeit less than doxorubicin, with the exception of CuAIsI-1 in AsPC-1 cells. Due to the short half-lives of ROS, it is possible that the CuAIsI-1 associated increase in ROS levels were high at a different time point following the initiation of treatment. However, the data are consistent with previously published studies which showed that apoptosis occurred in copper complex treated cells irrespective of high levels of ROS [44,49].

The induction of high levels of ROS in cancer cells leading to irreparable DNA and mitochondrial damage followed by the induction of apoptosis is a valuable treatment strategy in cancer treatment. ROS has been reported to trigger the intrinsic apoptotic pathway by increasing the permeability of the mitochondrial membrane and by inhibiting the anti-apoptotic protein Bcl-2 in human lung epithelial cancer cells and oral squamous carcinoma cells [72,73]. We therefore evaluated the effects of the copper complexes on mitochondrial integrity and its ability to activate caspase-9, the initiator caspase of the intrinsic apoptotic pathway.

The electrochemical gradient formed by the formation of ATP in the mitochondria contributes to the MMP that exists across the mitochondrial membranes [74]. Consequently, the status of MMP is a key indicator of mitochondrial health. A decrease in MMP indicates a disruption in mitochondrial activity and decreased ATP production, decreasing cell viability [74]. When MMP decreases, the mitochondrial permeability transition pore opens, allowing the release of pro-apoptotic proteins like cytochrome c, Smac/DIABLO and HtrA2/Omi [75]. Additionally, the release of apoptosis inducing factor (AIF) is dependent on the disruption of MMP [75]. Thus, loss of MMP is a prerequisite and preliminary indicator of intrinsic apoptosis [76].

In this study we used the JC-1 dye as an indicator of mitochondrial health. In healthy cells with an intact MMP, the JC-1 dye is present as a dimer showing as red fluorescing J-aggregates. In depolarized mitochondria, the JC-1 dye does not form dimers, with the monomeric species showing green fluorescence [59]. In untreated AsPC-1 and MIA

PaCa-2 cells, accumulation of red J-aggregates was seen, indicating active mitochondria. All the copper complexes and doxorubicin decreased the red fluorescence whereby the mitochondria of treated cells were visible as green fluorescence, indicating a complete loss in MMP. In AsPC-1 cells treated with Cu8AqN, CuPhTh₂ and CuAISI-1, most of the cells showed punctate green fluorescence, indicating structurally intact mitochondria. In contrast, cells treated with CuAISI-6 had diffuse green fluorescence, indicating loss of mitochondrial integrity [77].

All the copper complexes were able to activate caspase-9 which is the initiator caspase of the intrinsic/mitochondrial apoptotic pathway [78]. After a 48-h treatment with the test compounds, the copper complexes caused a statistically significant increase in active caspase-9 in both cell lines. In AsPC-1 cells, Cu8AqN and CuAISI-1 were the strongest activators, followed by CuAISI-6, while CuPhTh₂ was the weakest. In MIA PaCa-2 cells, CuPhTh₂ and Cu8AqN were the strongest activators of caspase-9, followed by CuAISI-1. Doxorubicin effectively activated caspase-9 in both cell lines. The activation of caspase-9 in both cell lines, albeit at various efficacies, indicates that the copper complexes were able to cause cell death via the activation of the intrinsic apoptotic pathway.

PDAC cells are known for their resistance to death-receptor mediated apoptosis [79]. Fas-associated phosphatase-1 is overexpressed in PDAC cells and renders pancreatic carcinoma cells resistant to Fas-initiated apoptosis by inhibiting the activation of caspase-8 and preventing the formation of the death inducing signaling complex, commonly referred to as DISC [79]. PDAC cells are classified as type II cells, meaning they require mitochondrial amplification pathways to induce apoptosis [80]. The copper complexes and doxorubicin were effective inducers of intrinsic apoptosis in both cell lines which is in line with these observations.

The activation of caspase-3 and/or caspase-7 is the endpoint of both the intrinsic and extrinsic apoptotic pathways. These active caspases are executioner caspases that cause nuclear fragmentation by cleaving inhibitor of caspase-activated DNase (ICAD). This in turn activates caspase-activated DNase (CAD) which ultimately causes DNA fragmentation. Active caspase-3 is primarily located in the nucleus [81,82]. In AsPC-1 cells the complexes were effective activators of caspase-3 activity confirming apoptosis as the primary mechanism of cell death, with the exception of CuAISI-1 which was a poor activator at the selected timepoint in the study.

Under the same treatment conditions, the copper complexes demonstrated higher caspase-3/7 activation in MIA PaCa-2 cells than in AsPC-1 cells. This was in line with annexin-V findings and cell morphology evaluation that demonstrated that late apoptotic cells are more frequently observed in MIA PaCa-2 cells compared to AsPC-1 cells. Additionally, the copper complexes induced ROS more potently in MIA PaCa-2 cells than in AsPC-1 cells. The data suggested that MIA PaCa-2 cells were more sensitive to the copper complexes than AsPC-1 cells and entered apoptosis more readily.

4.3. The copper complexes increased nuclear HMOX1 expression levels

In normal cells HMOX1 is found in the cytoplasm, anchored to the membrane of the smooth endoplasmic reticulum. Certain disease states induce HMOX1 translocation to the mitochondria, plasma membrane and the nucleus. Its enzymatic activity is preserved in all compartments except in the nucleus [83]. In both cell lines the four copper complexes caused a significant increase in HMOX1 protein expression which was primarily located in the nucleus. Western blotting data indicated that CuPhTh₂ was the most potent inducer of HMOX1 in both cell lines. The western blot data in this study indicated a molecular mass of 32 kDa for HMOX1 which implies the presence of a full-length, active enzyme. Currently the function of nuclear HMOX1 remains unresolved and it is not known if it may affect gene transcription. A study on mouse embryonic fibroblasts has shown that HMOX1 translocated to the nucleus

in response to hypoxia and was associated with the up-regulation of transcription factors involved in oxidative stress [84]. These transcription factors included AP-1, AP-2, Brn-3 and Core Binding Factor all which play a role in cell proliferation and differentiation [84]. The same study observed a decrease in the binding of nuclear factor kappa B (NF- κ B) to DNA [84]. It is widely accepted that increased HMOX1 expression protects tumour cells against oxidative stress [85], inflammatory mediators and apoptosis and promotes angiogenesis in these cells [86–88]. High levels of HMOX1 mRNA expression are associated with a significantly worse prognosis for lung, brain, breast, colorectal and haematological cancers, as predicted by a meta-analysis database [89].

In pancreatic cancer an increase in HMOX1 expression in patient samples, measured during chemotherapy, was associated with treatment failure [90]. It is thus important to evaluate the effect of investigational compounds on HMOX1 expression. In PDAC, HMOX1 expression has been reported to increase after chemotherapy and is associated with treatment failure [90,91].

Cytotoxicity studies were performed in the presence of a fixed concentration of a HMOX1 selective imidazole-based inhibitor, OB24. The data indicated a significant decrease in the IC₅₀ values of all the copper complexes, with those of the aromatic isoindolines reaching the nanomolar range. Thus, inhibition of HMOX1 increases the efficacy of the copper complexes indicating the potential benefit of HMOX1 inhibition in PDAC.

Due to the importance of the basic physiological functions of HMOX1, its inhibition, with the aim for clinical use, has not been actively investigated. Current HMOX1 inhibitors are metabolites of the haem pathway or involved in haem homeostasis, making them unsuitable drug candidates. To our knowledge, OB24 is the only commercially available small molecule HMOX1 inhibitor. In a study by Mucha et al., (2019) [92], another imidazole-based HMOX1 inhibitor was synthesized which showed positive responses in pre-clinical evaluations.

Western blot studies that isolated cytoplasmic and nuclear fractions of cells demonstrated an increase in nuclear HMOX1 following treatment of MIA PaCa-2 cells with nab-paclitaxel/gemcitabine, indicating nuclear translocation of HMOX1 [90]. The nuclear HMOX1 contributed to the cells' resistance to chemotherapy treatment [90]. In addition, the formation of ROS is associated with the induction of HMOX1. Our data indicates a poor correlation between HMOX1 induction and ROS formation suggesting that an in-depth investigation is warranted. Based on the results of the current study we propose that it would be advantageous to further investigate the use of non-toxic HMOX1 inhibitors as an adjunct to chemotherapeutic regimens in pancreatic and other cancers.

5. Conclusion

In this study, copper complexed with aromatic isoindoline ligands demonstrated superior activity compared to 8-aminoquinolone-naphthyl and phenanthroline-theophylline complexes. Both CuAISI-1 and CuAISI-6 complexes activated the intrinsic apoptotic pathway, with CuAISI-6 showing the highest activity. Compared to CuPhTh₂, the CuAISI complexes were less potent inducers of HMOX1, which is advantageous. Furthermore, the inhibition of HMOX1 led to a substantial increase in the potency of all four the complexes. This finding underscores the importance of evaluating the effects of investigational compounds for cancer treatment on HMOX1 induction, as it may be detrimental to cancer patients.

To our knowledge, these copper complexes compare favourably in efficacy with a wide range of published data on the anticancer effects of copper complexes, suggesting their potential as anticancer agents. The data presented here are encouraging and suggest that these complexes warrant further preclinical investigation. Additionally, our findings reinforce the evidence in the scientific literature that HMOX1 induction is an important consideration in cancer chemotherapy, and that its selective inhibition may enhance patient outcomes.

CRedit authorship contributions

Zakeeya Jhetam Data curation, Formal analysis, Investigation.

Leonie Harmse Conceptualization, Formal analysis, Validation, Supervision, Writing original draft and editing.

Carla Martins-Furness Formal analysis, Methodology, Validation, Writing original draft and editing.

Marietha Nel Formal analysis, Validation, Writing original draft.

Cathy Slabber Investigation, Methodology, Data curation, Validation, Writing original draft and editing.

Orde Q. Munro Conceptualisation, Funding acquisition, Resources.

Funding

This work was supported by the University of the Witwatersrand Faculty of Health Science Research Committee and the McGill Bequest to the Pharmacology Division. This work is also based on research supported by the South African Research Chairs Initiative of the Department of Science and Innovation (DSI) and National Research Foundation (NRF) of South Africa (Grant No 64799, OQM).

Declaration of competing interest

No competing interests to declare.

Data availability

Data will be made available on request.

Appendix A. Supplementary data

Supplementary data to this article can be found online at <https://doi.org/10.1016/j.jinorgbio.2024.112815>.

References

- [1] M. De La Cruz, S.D. Young, M.T. Ruffin, Diagnosis and management of pancreatic cancer, *Am. Fam. Physician* 89 (8) (2014) 626–632.
- [2] WHO., International Agency for Research on Cancer, Pancreas Cancer Facts Sheet. <https://gco.iarc.fr/today/data/factsheets/cancers/13-Pancreas-fact-sheet.pdf>, 2022. Accessed February 2024.
- [3] M. Pai, D. Spalding, Pancreatic cancer, *Med. J.* 43 (6) (2015) 329–333, <https://doi.org/10.1016/j.mpmed.2015.03.001>.
- [4] American Cancer Society, Cancer Facts & Figures 2024, American Cancer Society, Atlanta, 2024. <https://www.cancer.org/content/dam/cancer-org/research/cancer-facts-and-statistics/annual-cancer-facts-and-figures/2024/2024-cancer-facts-and-figures-acf.pdf>. Accessed February 2024.
- [5] D.A. Tuveson, J.P. Neoptolemos, Understanding metastasis in pancreatic cancer: a call for new clinical approaches, *Cell* 148 (1) (2012) 21–23, <https://doi.org/10.1016/j.cell.2011.12.021>.
- [6] Y. Qian, Y. Gong, Z. Fan, G. Luo, Q. Huang, S. Deng, et al., Molecular alterations and targeted therapy in pancreatic ductal adenocarcinoma, *J. Hematol. Oncol.* 13 (1) (2020) 130, <https://doi.org/10.1186/s13045-020-00958-3>.
- [7] A.M. Waters, C.J. Der, KRAS: the critical driver and therapeutic target for pancreatic cancer, *Cold Spring Harb. Perspect. Med.* 8 (9) (2018) a031435, <https://doi.org/10.1101/cshperspect.a031435>.
- [8] D.K. Podolsky, Chapter 31: neoplasia of the gastrointestinal tract, in: *Yamada's Textbook of Gastroenterology*, John Wiley and Sons Ltd, West Sussex, 2016.
- [9] C.A. Iacobuzio-Donahue, V.E. Velculescu, C.L. Wolfgang, R.H. Hruban, Genetic basis of pancreas cancer development and progression: insights from whole-exome and whole-genome sequencing, *Clin. Cancer Res.* 18 (16) (2012) 4257–4265, <https://doi.org/10.1158/1078-0432.CCR-12-0315>.
- [10] M. Serrano, G.J. Hannon, D. Beach, A new regulatory motif in cell-cycle control causing specific inhibition of cyclin D/CDK4, *Nature* 366 (6456) (1993) 704–707, <https://doi.org/10.1038/366704a0>.
- [11] R.M. Paranal, L.D. Wood, A.P. Klein, N.J. Roberts, Understanding familial risk of pancreatic ductal adenocarcinoma, *Fam. Cancer* 23 (4) (2024) 419–428, <https://doi.org/10.1007/s10689-024-00383-2>.
- [12] M. Schutte, R.H. Hruban, J. Gerads, R. Maynard, W. Hilgers, S.K. Rabindran, et al., Abrogation of the Rb/p16 tumor-suppressive pathway in virtually all pancreatic carcinomas, *Cancer Res.* 57 (15) (1997) 3126–3130.
- [13] N. Waddell, M. Pajic, A.M. Patch, D.K. Jang, K.S. Kassahn, P. Bailey, et al., Whole genomes redefine the mutational landscape of pancreatic cancer, *Nature* 518 (7540) (2015) 495–501, <https://doi.org/10.1038/nature14169>.
- [14] P.A.J. Muller, K.H. Vousden, Mutant p53 in cancer: new functions and therapeutic opportunities, *Cancer Cell* 25 (3) (2014) 304–317, <https://doi.org/10.1016/j.ccr.2014.01.021>.
- [15] I.A. Voutsadakis, Mutations of p53 associated with pancreatic cancer and therapeutic implications, *Ann. Hepatobiliary Pancreat. Surg.* 25 (3) (2021) 315–327, <https://doi.org/10.14701/ahbps.2021.25.3.315>.
- [16] H. Hu, Z. Ye, Y. Qin, X.W. Wu, X.J. Yu, Q.F. Zhuo, et al., Mutations in key driver genes of pancreatic cancer: molecularly targeted therapies and other clinical implications, *Acta Pharmacol. Sin.* 42 (11) (2021) 1725–1741, <https://doi.org/10.1038/s41401-020-00584-2>.
- [17] A.J. McCarthy, R. Chetty, Smad4/DPC4, *J. Clin. Pathol.* 71 (8) (2018) 661–664, <https://doi.org/10.1136/jclinpath-2018-205095>.
- [18] C.A. Iacobuzio-Donahue, DPC4 gene status of the primary carcinoma correlates with patterns of failure in patients with pancreatic cancer, *J. Clin. Oncol.* 27 (11) (2009) 1806–1813, <https://doi.org/10.1200/JCO.2008.17.7188>.
- [19] H.M. Kolbeinson, S. Chandana, G.P. Wright, M. Chung, Pancreatic cancer: a review of current treatment and novel therapies, *J. Investig. Surg.* 36 (1) (2023) 2129884, <https://doi.org/10.1080/08941939.2022.2129884>.
- [20] M. Manrai, T.V.S.V.G.K. Tilak, S. Dawra, S. Srivastava, A. Singh, Current and emerging therapeutic strategies in pancreatic cancer: challenges and opportunities, *World J. Gastroenterol.* 27 (39) (2021) 6572–6589, <https://doi.org/10.3748/wjg.v27.i39.6572>.
- [21] D.R. Principe, P.W. Underwood, M. Korc, J.G. Trevino, H.G. Munshi, A. Rana, The current treatment paradigm for pancreatic ductal adenocarcinoma and barriers to therapeutic efficacy, *Front. Oncol.* 11 (2021) 688377, <https://doi.org/10.3389/fonc.2021.688377>.
- [22] M.A. Tempero, M.P. Malafa, M. Al-Hawary, S.W. Behrman, A.B. Benson, D. B. Cardin, et al., Pancreatic adenocarcinoma, version 2. 2021, NCCN clinical practice guidelines in oncology, *J. Natl. Compr. Cancer Netw.* 19 (4) (2021) 439–457, <https://doi.org/10.6004/jnccn.2021.0017>.
- [23] M.H. Storaand, N. Tran, N. Martin, A. Jatoi, Pembrolizumab near the end of life in patients with metastatic pancreatic cancer: a multi-site consecutive series to examine survival and patient treatment burden, *Cancer Immunol. Immunother.* 72 (7) (2023) 2515–2520, <https://doi.org/10.1007/s00262-023-03397-4>.
- [24] N.J. Wheate, S. Walker, G.E. Craig, R. Oun, The status of platinum anticancer drugs in the clinic and in clinical trials, *Dalton Trans.* 39 (2010) 8113–8127, <https://doi.org/10.1039/C0DT00292E>.
- [25] S. Ivo, R. Dringen, J.F.B. Mercer, Copper: effects of deficiency and overload, *Met. Ions Life Sci.* 13 (2013) 359–387, <https://doi.org/10.1007/978-94-007-7500-8-11>.
- [26] P.J. Kennelly, Chapter 10. The biochemical roles of transition metals, in: P. J. Kennelly, K.M. Botham, O.P. McGuinness, V.W. Rodwell, P. Weil (Eds.), *Harper's Illustrated Biochemistry*, 32nd edition, McGraw Hill LLC, USA, 2023.
- [27] X. Tang, Z. Yan, Y. Miao, W. Ha, Z. Li, L. Yang, et al., Copper in cancer: from limiting nutrient to therapeutic target, *Front. Oncol.* 13 (2023) 1209156, <https://doi.org/10.3389/fonc.2023.1209156>.
- [28] L.M. Balsa, E.J. Baran, I.E. León, Copper complexes as antitumor agents: in vitro and in vivo evidence, *Curr. Med. Chem.* 30 (5) (2023) 510–557, <https://doi.org/10.2174/092986732866621117094550>.
- [29] C. Santini, M. Pellei, V. Gandin, M. Porchia, F. Tisato, C. Marzano, Advances in copper complexes as anticancer agents, *Chem. Rev.* 114 (1) (2014) 815–862, <https://doi.org/10.1021/cr400135x>.
- [30] P. Levín, M.C. Ruiz, A.I.B. Romo, O.R. Nascimento, A.L. Di Virgilio, A.G. Oliver, et al., Water-mediated reduction of [Cu(dmp)2(CH3CN)]₂+: implications of the structure of a classical complex on its activity as an anticancer drug, *Inorg. Chem. Front.* 8 (13) (2021) 3238–3252, <https://doi.org/10.1039/d1qi00233c>.
- [31] M.C. Ruiz, K. Perelmutter, P. Levín, A.I.B. Romo, L. Lemus, M.B. Fogolin, et al., Antiproliferative activity of two copper (II) complexes on colorectal cancer cell models: impact on ROS production, apoptosis induction and NF-kappaB inhibition, *Eur. J. Pharm. Sci.* 1 (169) (2022) 106092, <https://doi.org/10.1016/j.ejps.2021.106092>.
- [32] M.S. Sinicropi, J. Ceramella, D. Iacopetta, A. Catalano, A. Mariconda, C. Rosano, et al., Metal complexes with Schiff bases: data collection and recent studies on biological activities, *Int. J. Mol. Sci.* 23 (23) (2022) 14840, <https://doi.org/10.3390/ijms232314840>.
- [33] N. Kordestani, H.A. Rudbari, A.R. Fernandes, L.R. Raposo, A. Luz, P.V. Baptista, et al., Copper(II) complexes with tridentate halogen-substituted Schiff base ligands: synthesis, crystal structures and investigating the effect of halogenation, leaving groups and ligand flexibility on antiproliferative activities, *Dalton Trans.* 50 (11) (2021) 3990–4007, <https://doi.org/10.1039/d0dt03962d>.
- [34] M. Jiang, Q. Yan, Y. Fu, L. Meng, S. Gai, X. Pan, et al., Development of Cu(II) 4-hydroxybenzoylhydrazone complexes that induce mitochondrial DNA damage and mitochondria-mediated apoptosis in liver cancer, *Inorg. Biochem.* 256 (2024) 112550, <https://doi.org/10.1016/j.jinorgbio.2024.112550>.
- [35] A.Q. Liao, J. Wen, J.C. Wei, B.B. Xu, N. Jin, H.Y. Lin, et al., Syntheses, crystal structures of copper (II)-based complexes of sulfonamide derivatives and their anticancer effects through the synergistic effect of anti-angiogenesis, anti-inflammation, pro-apoptosis and cuproptosis, *Eur. J. Med. Chem.* 280 (2024) 116954, <https://doi.org/10.1016/j.ejmech.2024.116954>.
- [36] R. Galindo-Murillo, J.C. García-Ramos, L. Ruiz-Azuara, T.E. Cheatham 3rd, F. Cortés-Guzmán, Intercalation processes of copper complexes in DNA, *Nucleic Acids Res.* 43 (11) (2015) 5364–5376, <https://doi.org/10.1093/nar/gkv467>.
- [37] I. Carreira-Barral, M. Riopedre-Fernández, A. de Blas, J. Mosquera, M.E. Vázquez, Platas-Iglesias, et al., Ditopic binuclear copper(II) complexes for DNA cleavage, *J. Inorg. Biochem.* 205 (2020) 110995, <https://doi.org/10.1016/j.jinorgbio.2020.110995>.

- [38] C. Molinaro, N. Wambang, S. Pellegrini, N. Henry, M.F. Lensink, E. Germain, et al., Synthesis and biological activity of a new indenoisoquinoline copper derivative as a topoisomerase I inhibitor, *Int. J. Mol. Sci.* 24 (19) (2023) 14590, <https://doi.org/10.3390/ijms241914590>.
- [39] X. Chen, Q.P. Dou, J. Liu, D. Tang, Targeting ubiquitin-proteasome system with copper complexes for cancer therapy, *Front. Mol. Biosci.* 8 (2021) 649151, <https://doi.org/10.3389/fmolb.2021.649151>.
- [40] K.G. Daniel, P. Gupta, R.H. Harbach, W.C. Guida, Q.P. Dou, Organic copper complexes as a new class of proteasome inhibitors and apoptosis inducers in human cancer cells, *Biochem. Pharmacol.* 67 (6) (2004) 1139–1151, <https://doi.org/10.1016/j.bcp.2003.10.031>.
- [41] M. Carcelli, M. Tegoni, J. Bartoli, C. Marzano, G. Pelosi, M. Salvalajo, et al., In vitro and in vivo anticancer activity of tridentate thiosemicarbazone copper complexes: unravelling an unexplored pharmacological target, *Eur. J. Med. Chem.* 94 (2020) 112266, <https://doi.org/10.1016/j.ejmech.2020.112266>.
- [42] E. Ramachandran, V. Gandin, R. Bertani, P. Sgarbossa, K. Natarajan, N.S. P. Bhuvanesh, et al., Synthesis, characterization and biological activity of novel Cu (II) complexes of 6-methyl-2-oxo-1,2-dihydroquinoline-3-carbaldehyde-4n-substituted thiosemicarbazones, *Molecules* 25 (8) (2020) 1868, <https://doi.org/10.3390/molecules25081868>.
- [43] L.M. Balsa, M.R. Rodriguez, V. Ferraresi-Curotto, B.S. Parajón-Costa, A. C. Gonzalez-Baró, I.E. León, Finding new molecular targets of two copper(II)-hydrazone complexes on triple-negative breast cancer cells using mass-spectrometry-based quantitative proteomics, *Int. J. Mol. Sci.* 24 (8) (2023) 7531, <https://doi.org/10.3390/ijms24087531>.
- [44] L. Harmse, N. Gangat, C. Martins-Furness, J. Dam, C.B. de Koning, Copper-imidazo [1,2-a]pyridines induce intrinsic apoptosis and modulate the expression of mutated p53, haem-oxygenase-1 and apoptotic inhibitory proteins in HT-29 colorectal cancer cells, *Apoptosis J.* 24 (7–8) (2019) 623–643, <https://doi.org/10.1007/s10495-019-01547-7>.
- [45] M. Pellei, L. Bagnarelli, L. Luciani, F. Del Bello, G. Giorgioni, A. Piergentili, et al., Synthesis and cytotoxic activity evaluation of new Cu(I) complexes of bis(pyrazol-1-yl) acetate ligands functionalized with an NMDA receptor antagonist, *Int. J. Mol. Sci.* 21 (7) (2020) 2616, <https://doi.org/10.3390/ijms21072616>.
- [46] S. Barrett, M. De Franco, A. Kellet, E. Dempsey, C. Marzano, A. Erxleben, et al., Anticancer activity, DNA binding and cell mechanistic studies of estrogen-functionalised Cu(II) complexes, *J. Biol. Inorg. Chem.* 1 (2020) 49–60, <https://doi.org/10.1007/s00775-019-01732-8> (Epub 2019 Oct 26).
- [47] S.C. Howard, D.P. Jones, C.-H. Pui, The tumor lysis syndrome, *N. Engl. J. Med.* 364 (19) (2011) 1844–1854, <https://doi.org/10.1056/NEJMr0904569>.
- [48] J. Dam, Z. Ismail, T. Kurebwa, N. Gangat, L. Harmse, H.M. Marques, et al., Synthesis of copper and zinc 2-(pyridin-2-yl)imidazo[1,2-a]pyridine complexes and their potential anticancer activity, *Eur. J. Med. Chem.* 126 (2017) 353–368, <https://doi.org/10.1016/j.ejmech.2016.10.041>.
- [49] Z. Ismail, J. Dam, C. Penny, C.B. de Koning, L. Harmse, Copper-imidazo[1,2-a]pyridines differentially modulate pro- and anti-apoptotic protein and gene expression in HL-60 and K562 leukaemic cells to cause apoptotic cell death, *Biochim. Biophys. Acta, Mol. Cell Res.* 1869 (1) (2022) 119160, <https://doi.org/10.1016/j.bbamcr.2021.119160>.
- [50] P.O. Berberat, Z. Dambrauskas, A. Gulbinas, T. Giese, N. Giese, B. Künzli, et al., Inhibition of heme oxygenase-1 increases responsiveness of pancreatic cancer cells to anticancer treatment, *Clin. Cancer Res.* 11 (10) (2005) 3790–3798, <https://doi.org/10.1158/1078-0432.CCR-04-2159>.
- [51] M. Sunamura, D.G. Duda, M.H. Ghattas, L. Lozonchi, F. Motoi, J. Yamauchi, et al., Heme oxygenase-1 accelerates tumor angiogenesis of human pancreatic cancer, *Angiogenesis* 6 (1) (2003) 15–24, <https://doi.org/10.1023/a:1025803600840>.
- [52] M. Miyake, K. Fujimoto, S. Anai, S. Ohnishi, M. Kuwada, Y. Nakai, et al., Heme oxygenase-1 promotes angiogenesis in urothelial carcinoma of the urinary bladder, *Oncol. Rep.* 25 (3) (2011) 653–660, <https://doi.org/10.3892/or.2010.1125>.
- [53] L.E. Otterbein, A.M. Choi, Heme oxygenase: colors of defense against cellular stress, *Am. J. Phys. Lung Cell. Mol. Phys.* 279 (2000) L1029–L1037, <https://doi.org/10.1152/ajplung.2000.279.6.L1029>.
- [54] N. Myeza, C. Slabber, O.Q. Munro, S. Sookai, S.C. Zacharias, C. Martins-Furness, et al., An 8-aminoquinoline-naphthyl copper complex causes apoptotic cell death by modulating the expression of apoptotic regulatory proteins in breast cancer cells, *Eur. J. Pharmacol.* 978 (2024) 176764, <https://doi.org/10.1016/j.ejphar.2024.176764>.
- [55] A.T. Gordon, O.O. Abosedo, S. Ntsimango, E.C. Hosten, N. Myeza, A. Van Eyk, et al., Synthesis and anticancer evaluation of copper(II)- and manganese(II)-theophylline mixed ligand complexes, *Polyhedron* 214 (2022) 115649, <https://doi.org/10.1016/j.poly.2022.115649>.
- [56] A.W. Addison, P.J. Burke, Synthesis of some imidazole- and pyrazole- derived chelating agents, *J. Heterocyclic Chem.* 18 (4) (1981) 803–805, <https://doi.org/10.1002/jhet.5570180436>.
- [57] W.O. Siegl, Metal ion activation of nitriles. Syntheses of 1,3-bis(aryl)imino isoindolines, *J. Org. Chem.* 42 (11) (1977) 1872–1878, <https://doi.org/10.1021/J000431A011>.
- [58] T. Mosmann, Rapid colorimetric assay for cellular growth and survival: application to proliferation and cytotoxicity assays, *J. Immunol. Methods* 65 (1–2) (1983) 55–63, [https://doi.org/10.1016/0022-1759\(83\)90303-4](https://doi.org/10.1016/0022-1759(83)90303-4).
- [59] M. Reers, T.W. Smith, L.B. Chen, J-aggregate formation of a carbocyanine as a quantitative fluorescent indicator of membrane potential, *Biochemistry* 30 (18) (1991) 4480–4486, <https://doi.org/10.1021/bi00232a015>.
- [60] A. Pierzyńska-Mach, P.A. Janowski, J.W. Dobrucki, Evaluation of acridine orange, LysoTracker Red, and quinacrine as fluorescent probes for long-term tracking of acidic vesicles, *Cytometry A* 85 (8) (2014) 729–737, <https://doi.org/10.1002/cyto.a.22495>.
- [61] C.A. Juan, J.M. Pérez de la Lastra, F.J. Plou, E. Pérez-Lebeña, The chemistry of reactive oxygen species (ROS) revisited: outlining their role in biological macromolecules (DNA, lipids and proteins) and induced pathologies, *Int. J. Mol. Sci.* 22 (9) (2021) 4642, <https://doi.org/10.3390/ijms22094642>.
- [62] A. Wellstein, E.A. Sausville, Cytotoxics and antimetabolites, in: L.L. Brunton, B. C. Knollmann (Eds.), *Goodman and Gilman's: The Pharmacological Basis of Therapeutics*, 14th edition, McGraw-Hill Education, USA, 2023.
- [63] H. Nakamura, K. Takada, Reactive oxygen species in cancer: current findings and future directions, *Cancer Sci.* 112 (10) (2021) 3945–3952, <https://doi.org/10.1111/cas.15068>.
- [64] M.A. Alaoui-Jamali, T.A. Bismar, A. Gupta, W.A. Szarek, J. Su, W. Song, et al., A novel experimental heme oxygenase-1-targeted therapy for hormone-refractory prostate cancer, *Cancer Res.* 69 (20) (2009) 8017–8024, <https://doi.org/10.1158/0008-5472.CAN-09-0419>.
- [65] S. Toné, K. Sugimoto, K. Tanda, T. Suda, K. Uehira, H. Kanouchi, et al., Three distinct stages of apoptotic nuclear condensation revealed by time-lapse imaging, biochemical and electron microscopy analysis of cell-free apoptosis, *Exp. Cell Res.* 313 (16) (2007) 3635–3644, <https://doi.org/10.1016/j.yexcr.2007.06.018>.
- [66] L. Galluzzi, J.M. Bravo-San Pedro, I. Vitale, S.A. Aaronson, J.M. Abrams, D. Adam, et al., Essential versus accessory aspects of cell death: recommendations of the NCCD 2015, *Cell Death Differ.* 22 (1) (2015) 58–73, <https://doi.org/10.1038/cdd.2014.137>.
- [67] L. Galluzzi, G. Kroemer, Secondary necrosis: accidental no more, *Trends Cancer* 3 (1) (2017) 1–2, <https://doi.org/10.1016/j.trecan.2016.12.001>.
- [68] M. Salimi, K. Abdi, H.M. Kandelous, H. Hadadzadeh, K. Azadmanesh, A. Amanzadeh, et al., Antiproliferative effects of copper(II)-polypyridyl complexes in breast cancer cells through inducing apoptosis, *BioMetals* 28 (2) (2015) 267–278, <https://doi.org/10.1007/s10534-015-9820-5>.
- [69] T. Ma, J. Xu, Y. Wang, H. Yu, Y. Yang, Y. Liu, et al., Ternary copper(II) complexes with amino acid chains and heterocyclic bases: DNA binding, cytotoxic and cell apoptosis induction properties, *J. Inorg. Biochem.* 144 (2015) 38–46, <https://doi.org/10.1016/j.jinorgbio.2014.12.011>.
- [70] S.K. Bardaweel, M. Gul, M. Alzweiri, A. Ishaqat, H.A. Alsalamat, R.M. Bashatwah, Reactive oxygen species: the dual role in physiological and pathological conditions of the human body, *Eurasian J. Med.* 50 (3) (2018) 193–201, <https://doi.org/10.5152/eurasianjmed.2018.17397>.
- [71] A. Kirtonia, G. Sethi, M. Garg, The multifaceted role of reactive oxygen species in tumorigenesis, *Cell. Mol. Life Sci.* 77 (22) (2020) 4459–4483, <https://doi.org/10.1007/s00018-020-03536-5>.
- [72] S. Luanpitpong, P. Chanvorachote, C. Stehlik, W. Tse, P.S. Callery, L. Wang, et al., Regulation of apoptosis by Bcl-2 cysteine oxidation in human lung epithelial cells, *Mol. Biol. Cell* 24 (6) (2013) 858–869, <https://doi.org/10.1091/mbc.E12-10-0747>.
- [73] D. Li, E. Ueta, T. Kimura, T. Yamamoto, T. Osaki, Reactive oxygen species (ROS) control the expression of Bcl-2 family proteins by regulating their phosphorylation and ubiquitination, *Cancer Sci.* 95 (8) (2004) 644–650, <https://doi.org/10.1111/j.1349-7006.2004.tb03323.x>.
- [74] S. Sakamuru, M.S. Attene-Ramos, M. Xia, Mitochondrial membrane potential assay, *Methods Mol. Biol.* 1473 (2016) 17–22, https://doi.org/10.1007/978-1-4939-6346-1_2.
- [75] J.D. Ly, D.R. Grubb, A. Lawen, The mitochondrial membrane potential ($\Delta\psi_m$) in apoptosis: an update, *Apoptosis* 8 (2) (2003) 115–128, <https://doi.org/10.1023/A:1022945107762>.
- [76] M. Redza-Dutordoir, D.A. Averill-Bates, Activation of apoptosis signalling pathways by reactive oxygen species, *Biochim. Biophys. Acta* 1863 (12) (2016) 2977–2992, <https://doi.org/10.1016/j.bbamcr.2016.09.012>.
- [77] T. Zuliani, R. Duval, C. Jayat, S. Schnébert, P. André, M. Dumas, et al., Sensitive and reliable JC-1 and TOTO-3 double staining to assess mitochondrial transmembrane potential and plasma membrane integrity: interest for cell death investigations, *Cytometry A* 54A (2) (2003) 100–108, <https://doi.org/10.1002/cyto.a.10059>.
- [78] M.L. Würstle, M.A. Laussmann, M. Rehm, The central role of initiator caspase-9 in apoptosis signal transduction and the regulation of its activation and activity on the apoptosome, *Exp. Cell Res.* 318 (11) (2012) 1213–1220, <https://doi.org/10.1016/j.yexcr.2012.02.013>.
- [79] R. Hamacher, R.M. Schmid, D. Saur, G. Schneider, Apoptotic pathways in pancreatic ductal adenocarcinoma, *Mol. Cancer* 7 (2008) 64, <https://doi.org/10.1186/1476-4598-7-64>.
- [80] S. Westphal, H. Kalthoff, Apoptosis: targets in pancreatic cancer, *Mol. Cancer* 2 (2003) 6, <https://doi.org/10.1186/1476-4598-2-6>.
- [81] M. Enari, H. Sakahira, H. Yokoyama, K. Okawa, A. Iwamatsu, S. Nagata, A caspase-activated DNase that degrades DNA during apoptosis, and its inhibitor ICAD, *Nature* 391 (6662) (1998) 43–50, <https://doi.org/10.1038/34112>.
- [82] S. Elmore, Apoptosis: a review of programmed cell death, *Toxicol. Pathol.* 35 (2007) 495–516, <https://doi.org/10.1080/01926230701320337>.
- [83] S.K. Chiang, S.E. Chen, L.C. Chang, The role of HO-1 and its crosstalk with oxidative stress in cancer cell survival, *Cells* 10 (2021) 2401, <https://doi.org/10.3390/cells10092401>.
- [84] Q. Lin, S. Weis, G. Yang, Y.H. Weng, R. Helston, K. Rish, et al., Heme oxygenase-1 protein localizes to the nucleus and activates transcription factors important in oxidative stress, *J. Biol. Chem.* 282 (28) (2007) 20621–20633, <https://doi.org/10.1074/jbc.M607954200>.
- [85] X. Sun, S. Wang, J. Gai, J. Li, Y. Li, J. Zhao, et al., SIRT5 promotes cisplatin resistance in ovarian cancer by suppressing DNA damage in a ROS-dependent

- manner via regulation of the Nrf2/HO-1 pathway, *Front. Oncol.* 9 (2019) 754, <https://doi.org/10.3389/fonc.2019.00754>.
- [86] P. Podkalicka, O. Mucha, A. Józkowicz, J. Dulak, A. Łoboda, Heme oxygenase inhibition in cancers: possible tools and targets, *Contemp. Oncol.* 22 (1A) (2018) 23–32, <https://doi.org/10.5114/wo.2018.73879>.
- [87] M. Nitti, J. Ortolan, A.L. Furfaro, Role of heme oxygenase-1 in tumor immune escape, *Redox Exp. Med.* (1) (2023) e230006, <https://doi.org/10.1530/REM-23-0006cape>.
- [88] P. Banerjee, A. Basu, B. Wegiel, L.E. Otterbein, K. Mizumura, M. Gasser, et al., Heme oxygenase-1 promotes survival of renal cancer cells through modulation of apoptosis- and autophagy-regulating molecules, *J. Biol. Chem.* 287 (38) (2012) 32113–32123, <https://doi.org/10.1074/jbc.M112.393140>.
- [89] H. Wang, Q. Cheng, L. Bao, M. Li, K. Chang, X. Yi, Cytoprotective role of heme oxygenase-1 in cancer chemoresistance: focus on antioxidant, antiapoptotic, and pro-autophagy properties, *Antioxidants* 12 (2023) 1217, <https://doi.org/10.3390/antiox12061217>.
- [90] M.Y. Abdalla, I.M. Ahmad, S. Rachagani, K. Banerjee, C.M. Thompson, H. C. Maurer, et al., Enhancing responsiveness of pancreatic cancer cells to gemcitabine treatment under hypoxia by heme oxygenase-1 inhibition, *Transl. Res.* 207 (2019) 56–69, <https://doi.org/10.1016/j.trsl.2018.12.008>.
- [91] I.M. Ahmad, A.J. Dafferner, K.A. O'Connell, K. Mehla, B.E. Britigan, M. A. Hollingsworth, M.Y. Abdalla, Heme oxygenase-1 inhibition potentiates the effects of nab- paclitaxel-gemcitabine and modulates the tumor microenvironment in pancreatic ductal adenocarcinoma, *Cancers* 13 (9) (2021) 2264, <https://doi.org/10.3390/cancers13092264>.
- [92] O. Mucha, P. Podkalicka, M. Mikulski, S. Barwacz, K. Andrysiak, A. Biela, et al., Development and characterization of a new inhibitor of heme oxygenase activity for cancer treatment, *Arch. Biochem. Biophys.* 671 (2019) 130–142, <https://doi.org/10.1016/j.abb.2019.07.002>.